# General Disclaimer

One or more of the Following Statements may affect this Document

- This document has been reproduced from the best copy furnished by the organizational source. It is being released in the interest of making available as much information as possible.

- This document may contain data, which exceeds the sheet parameters. It was furnished in this condition by the organizational source and is the best copy available.

- This document may contain tone-on-tone or color graphs, charts and/or pictures, which have been reproduced in black and white.

- This document is paginated as submitted by the original source.

- Portions of this document are not fully legible due to the historical nature of some of the material. However, it is the best reproduction available from the original submission.

Produced by the NASA Center for Aerospace Information (CASI)
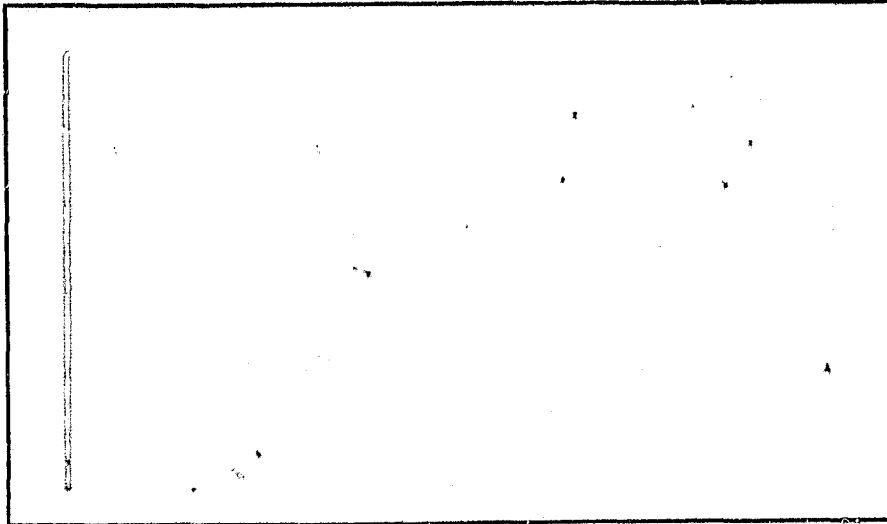
Contract 956034
Final Report

UNIVERSITY of PENNSYLVANIA

The Moore School of Electrical Engineering

PHILADELPHIA, PENNSYLVANIA 19104

ANALYSIS AND EVALUATION

IN THE PRODUCTION PROCESS

AND EQUIPMENT AREA

OF THE

LOW-COST SOLAR ARRAY PROJECT

Contract 956034
Final Report

April 30, 1982

M. Wolf

SUMMARY

The project began with techno-economic evaluations of MEPSDU processes, and then proceeded to a study of requirements for the longer range, potentially substantial improvement of the efficiency of Si solar cells.

Of the MEPSDU processes investigated, it was found that the Solarex metallization design and process selection should be modified to yield substantially higher output of the 10cm x 10cm cells, while the Westinghouse design is extremely close to the optimum. In addition, further attention to the Solarex pn junction and base high/low junction formation processes could be beneficial.

For the future efficiency improvement, it was found that refinement of the various minority carrier lifetime measurement methods is needed, as well as considerably increased sophistication in the interpretation of the results of these methods. In addition, it was determined that further experimental investigation of the Auger lifetime is needed, to conclusively determine the Auger coefficients for the direct Auger recombination at high majority carrier concentrations. This will determine the ultimately achievable efficiency of Si solar cells. If the Auger coefficients should be substantially lower than presently thought, more attention may have to be given to bandgap narrowing. Finally, more needs to be known about the effects of various device processes on the minority carrier lifetime ultimately existing in the diverse layers of the device.

Further, as one of the more frequently used methods for minority carrier lifetime measurement, the storage delay time (diode reverse recovery time) method was theoretically and experimentally investigated with respect to its limitations and its spurious effects which could lead to misinterpretation of the results. It was determined that two types of influences can alter the effects being measured and interpreted for the minority carrier lifetime of a given part of the sample:

influences from outside the part being measured (e.g. the base), such as excess currents due to recombination in depletion regions, or currents due to changes of the depletion layer charge in transient methods, and secondly influences from the respective part itself, such as surface recombination of the back surface of this layer. A great deal needs therefore to be known of the structure and characteristics of the sample to be tested, before any method can be successfully applied and its results appropriately interpreted. For the storage delay time method, these precautions have been delineated in more detail.

TABLE OF CONTENTS

LIST OF TABLES

LIST OF FIGURES

I. INTRODUCTION

This project started under the LSA program and continued under the FSA project. Consequently, it was originally more closely coupled to the MEPSDU program, with technical and economic assessments of the various process approaches, and a particular view towards the avoidance of unnecessary solar cell performance losses in the process sequences applied.

With the transition to the FSA program, the viewpoint shifted more towards future, larger efficiency improvements, and to the problems which stand in the way towards achieving these improvements. Consequently, attention was focused on the relationship between achievable minority carrier lifetimes and dopant concentration, with a particular view towards direct Auger recombination. As an outgrowth of this study, a closer look was taken at the problems and limitations of minority carrier lifetime measurement methods.

I.   ASSESSMENT OF MEPSDU PROCESSES.

A.   Processes of the Solarex MEPSDU Sequence.

The Solarex reports on the MEPSDU Contract DOE/JPL 955902 give indications that a considerable improvement of the processes selected for the MEPSDU sequence is possible. The aim of such improvement should be a substantial increase in cell efficiency, and consequently the module power output, while incurring not more than a moderate rise of the production costs. Thus, the cost-effectiveness of the process sequence could be significantly increased.

Three areas have been noted to merit closer investigation in this respect: the contact design and metallization process, the pn (front) junction formation process, and the high low (back) junction formation process.

1. Front Metallization.

In reviewing the Solarex MEPSDU cell design and process sequence, the item which seems to merit attention most is the front metallization system. According to the Solarex data[1] which upon cursory check appear correct, 0.337W are lost due to front metal shading (0.139W grid line shading and 0.032W bus line shading) and to ohmic losses (0.068W in the diffused region, 0.014 in the grid lines, and 0.084W in the bus lines), while the cell output is only 0.8-0.9W. This amounts to a loss, just due to the front metal design, of 27 to 30% of the potentially available cell output if the shading and ohmic losses would be zero.

Evidence of the insufficiency of the front contact pattern design and the metal selection is also contained in reference 2, which describes several metallization experiments on 10 cm x 10 cm semicrystalline cells which were co-diffused in lot 10C with 2 cm x 2 cm cells in a belt furnace. The small cells had TiPdAg metallization, the large cells the MEPSDU metallization process. Neither cells were AR coated. The small cells had an average efficiency of 6.7%, the large ones of 4.3%. Not all of this difference may be ascribed to the front metallization, since V_{oc} and j_{sc} also differed substantially. Also, as previously shown, using solder for the conduction layer has to be expensive, and is listed at $0.0216/W material content in reference 3. In addition, this pricing is based on 15% efficient encapsulated cells, which is not likely to be attained with such large shading and ohmic losses. A finer-line grid, and a copper conduction layer will be needed to attain combined shading and ohmic losses as low as 12% on such large cells (10 cm x 10 cm), and wire-built-up bus lines to reduce these losses further to about 5%. Of concern is also the relatively high contact resistance of 0.26 to 0.41 $\Omega \cdot cm^2$ [4], which should find further attention.

Additional questions on the quality of the metallization arise from the wide spread of the tab pull test data[5]

which ranged from a low of 100-200g (neglecting lower values from problem runs) to a high of about 1000 to 2000g, with standard deviations of about 300 to 500g. It is not clear from the report whether the cells were solder dipped before the pull-tests which could provide some effect of sintering and strengthening the contact, but could also add the beam strength of the thick solder layer to the tab solder joint. The contact quality may also be questioned on the basis of the somewhat large values of contact resistance found, although these might be based on problems with the measurement method.

2. PN-junction Formation Process.

The second area where further investigations might be fruitful, is that of pn-junction formation. The data presented[6,7] do not conclusively indicate that 890°C is the optimum diffusion temperature. In fact, temperatures lower than 890°C seem to provide a higher solar cell power output. In addition, the application of a metallization system with too high a series resistance tends to let a diffused layer of lower sheet resistance appear more favorable, than a more optimized metallization would. Lower diffused layer sheet resistance values are obtained at higher diffusion temperatures.

3. Base High/Low Junction Formation.

The final question concerns the optimization of the high/low (back) junction formation process.[8] The data given show only averages, obtained on single lots, and do not permit an evaluation of the statistical significance of the results. Including standard deviations and some repetition of the experiments helps to convey confidence in the process control achieved.

B. Processes of the Westinghouse MEPSDU Sequence.

1. Metallization.

As the Westinghouse fanned grid line pattern "appears so obviously wrong", with very dense grid-line placement in some areas, and very sparse placement in others (Fig. 1), it was thought to be interesting to evaluate the total losses connected with this front layer metallization design. It was first attempted to make some quick, first order approximations, but it turned out that their errors were too large for any credible estimation. Closer approximations had, therefore, to be made for both the grid line losses and the front layer (diffused layer) losses, while computations of the total available power and of the grid line shading losses were quite simple. For the front layer losses, two computations were carried out, involving different simplified current flow patterns. Except for the irregular shaped area below the shortest grid line (located nearest the edge with the interconnect pads), all equations have been derived.

The dimensions of the pattern have been scaled off a graph for the 2.5 cm x 9.8 cm cell.[9] For the sheet resistance of the diffused layer and for the dimensions of the grid lines, data were obtained from Westinghouse.[10] The sheet resistance of the diffused layer is 60 ohms. The grid line width is 25 μm, and their thickness is, on average, 8 μm.

a. Description of the Evaluation Method

The fanned grid line pattern as a whole is a periodic repetition of the pattern of a "unit cell". Each unit cell is symmetrical around its centerline which extends in the longitudinal direction of the unit cell. The pattern on each unit cell is the mirror image of the other, so that it is adequate to analyze a half-unit cell (Fig. 1). The areas on the diffused layer from which current is collected by the individual grid lines, are of triangular shape. In addition, the triangular collecting areas on the two sides of each metallic grid line are of different shapes (Fig. 2). It is therefore necessary

6

Approximate Westinghouse Grid Line Pattern.

ORIGINAL PAGE IS
OE POOR QUALITY

0.5

0.143 typ.
0.07

2.5

1.5

0.8

0.35

0.1

0.05

0.05
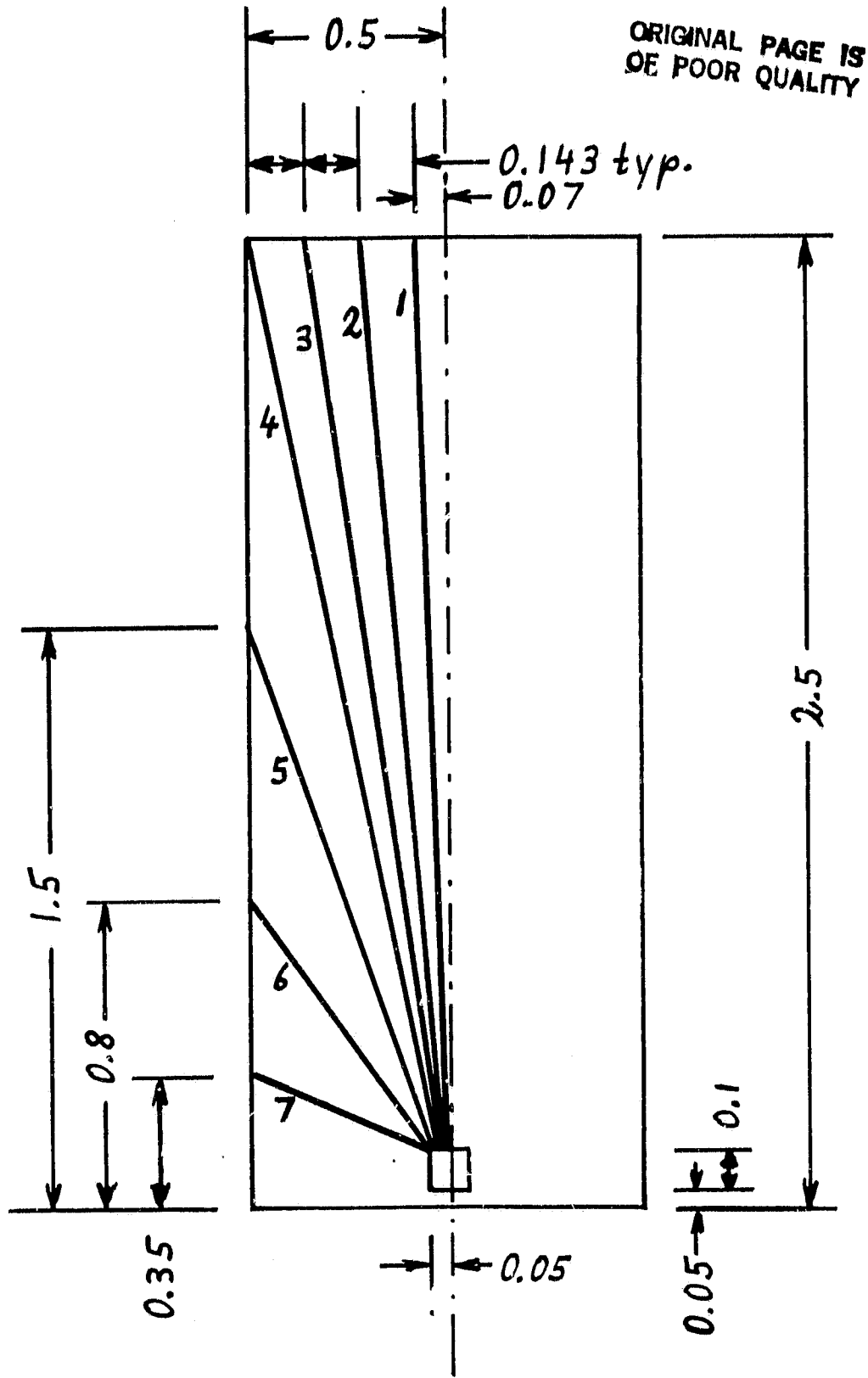
All dimensions in cm.

FIG. 1   7

h_1 h_2

edge of
unit field

triangle a
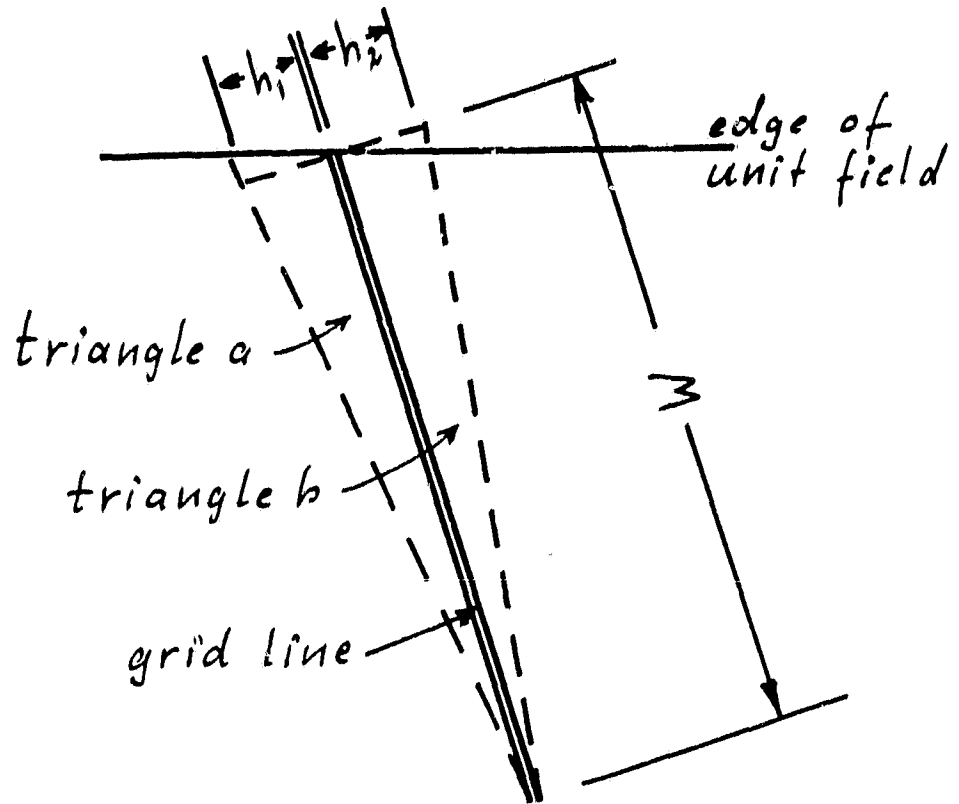
triangle b

grid line

FIG. 2

8

to evaluate the power loss separately for each triangular area of the diffused layer. It is simple to determine, for each grid line, the collecting area on the front layer. It is slightly more involved to determine the current distribution in the grid lines as function of distance from the interconnect attachment point. The current density entering the grid lines increases with distance from their attachment points up to a maximum near the far end of the grid lines, in contrast to the case of a parallel grid line pattern, where the entering current density is constant. The most difficult part is the determination of the power loss in the triangular (and one pentagon) shaped areas of the diffused layer.

aa. Determination of the Available Power

For the calculation of the available peak power, the approximate collecting areas on each side of the grid lines were calculated, and multiplied with the estimated maximum power current density j_{mp} of 30 mA cm^{-2} and maximum power voltage V_{mp} of 0.5V. The areas A were determined from

$$A = \frac{1}{2} b \cdot h ; \tag{1}$$

b being the length of the base of the triangle and h the length of its height. Thus, the available power is given by:

$$P_{avail} = \frac{1}{2} b \cdot h \cdot j_{mp} \cdot V_{mp} ; \tag{2}$$

ab. Grid Line Shading

The area shaded by a gridline is simply the product of the length of the grid line and its width T_{GL}. For the grid lines close to the centerline of the unit field, the angle between the centerline and the grid line is very small, so that the length of the grid line can be approximated by the longitudinal dimension W of the unit cell:

$$A_{GL} = W \cdot T_{GL} ; \tag{3}$$

ac. Determination of Joule Losses in the Grid Lines

To determine the current distribution I(x) in the grid lines, a fundamental assumption had to be made concerning the

current distribution in the diffused layer. It was assumed
that all current in the diffused layer flows normal to the grid
lines. This is strictly true in parallel grid line systems,
except near the juncture of the grid lines with a bus line. In
the triangular system, a slight current spreading towards the
interconnect attachment point should be expected. The effect
will be very small in the narrow triangles, but may be more
pronounced in the few triangles of greater height.

The fanned grid line pattern contains 2 types of trian-
gles (triangles a and b of Fig. 2). In triangles of type a,
some collecting area extends beyond the length of the grid line.
For this part of the collecting area, it has been assumed that
the current collected by it enters at the end of the grid line,
and that this excess current compensates the reduced current
entering the grid line from triangle b.

For a reasonable approximation, it is thus assumed that
both triangles are terminated by normal h to the grid line,
which is located at its end. The current density entering
the grid line at the distance x from the interconnect attachment
area from one of these triangles with height h_1 is then given by

$$I(x) = \int_x^W j_{mp} \frac{h_1}{W} x \, dx \qquad (4)$$

$$= j_{mp} \frac{h_1}{2W} \left(W^2 - x^2\right). \qquad (5)$$

The power dissipated in a grid line element of length dx is
given by:

$$dP_{GL} = I(x)^2 \, dR \, ; \qquad (6)$$

where

$$dR = R_{sh,GL} \cdot \frac{dx}{T_{GL}} \, ; \qquad (7)$$

10

with $R_{sh,GL}$ being the sheet resistance of the grid line metallization, and T_{GL} the grid line width. Thus, the total power dissipated in a grid line is:

$$P_{GL} = j_{mp}^2 R_{sh,GL} \frac{(h_1+h_2)^2}{4W^2 T_{GL}} \int_0^W \left(W^2 - x^2\right) dx \; ; \quad (8)$$

which includes the contribution from both triangles of heights h_1 and h_2, respectively. This yields

$$P_{GL} = \frac{2}{15} j_{mp}^2 R_{sh,GL} \frac{W^3}{T_{GL}} \left(h_1+h_2\right)^2 \; ; \quad\quad (9)$$

This compares with:

$$P_{GL} = \frac{1}{3} j_{mp}^2 R_{sh,GL} \frac{W^3}{T_{GL}} S^2 \; ; \quad\quad\quad (10)$$

for the parallel grid line of uniform width, with grid line spacing S.

ad. Determination of Joule Losses in the Front Layer

For the purpose of determining the Joule losses in the front (diffused) layer, two approximations to the actual value of this power loss were used. The more optimistic value resulting from these approximations has been used for the tabulation of the data.

The analytical problem arises from the shape of the collecting area, which results in a case in which the equi-potential lines will generally not be parallel to each other or to the grid line (Fig. 3). Consequently, the current flow which occurs normal to the equi-potential lines, will not be normal to the grid line along its whole length, as it is in the parallel grid line case. Making the assumption that the current flow would be normal to the grid line (Fig. 4), leads to a higher estimate of the power loss than will actually occur. In this triangular pattern, a current flow normal to the grid line would result in a very non-uniform current density along lines which are parallel to the grid lines. Consequently, the current will redistribute itself to paths which will be slightly longer, but which will result in a slightly more uniform current density (Fig. 3). As this case is mathematically difficult to treat and not analytically solvable, the first estimation method assumes current paths normal to the grid lines. In contrast, the second method assumes that the current spreads out uniformly along lines parallel to the grid lines (Fig. 5). The second method yields the lower estimates of the power loss.

In the first approximation model, the current flow in a strip of width dx of the front layer (diffused layer), oriented normal to the grid line and located at the distance x from the attachment point of the grid line, is given by:

$$I_{mp}(x,y) = j_{mp}(\ell - y) \, dx \; ; \qquad (11)$$

The incremental power dissipated in the length element dy located at y in this strip of front layer with the sheet resistance $R_{sh,FL}$ is:
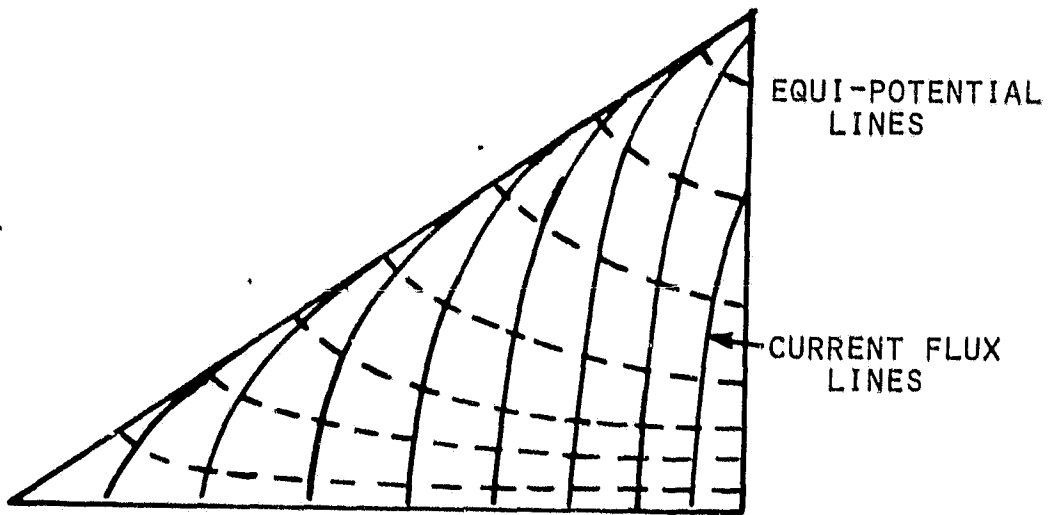
EQUI-POTENTIAL
LINES

CURRENT FLUX
LINES

FIG. 3

13

FIG. 4

b.)

a.)

FIG. 5

15
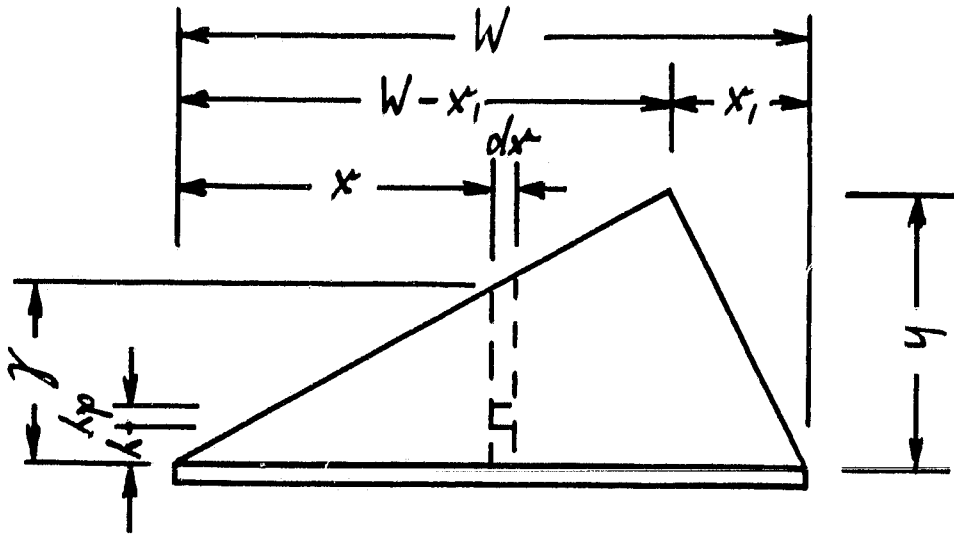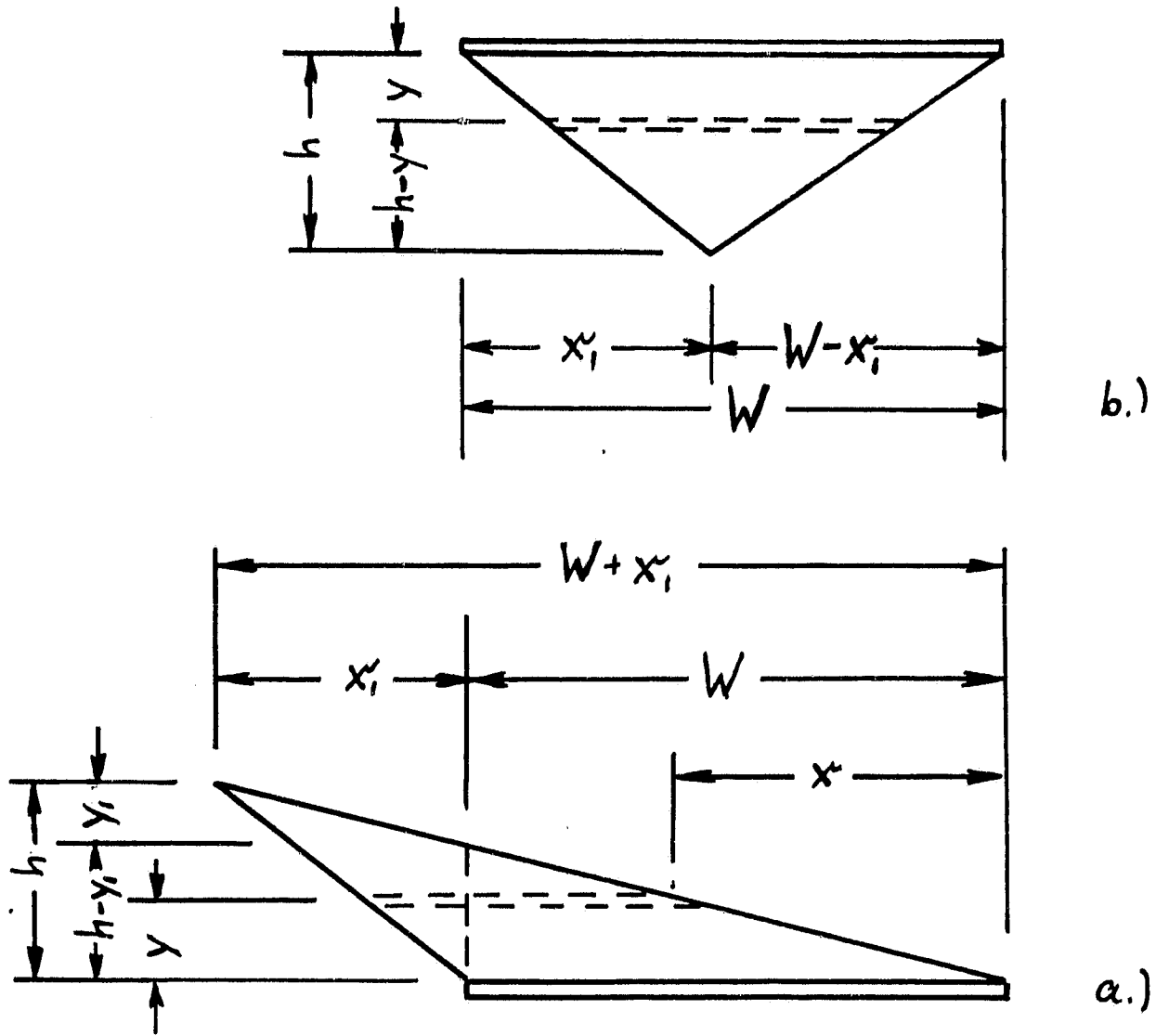
$$dP_{FL} = I^2(x,y) \cdot dR_{FL} ;$$

$$= j_{mp}^2 (\ell - y)^2 dx^2 \cdot R_{sh,FL} \cdot \frac{dy}{dx} ; \qquad (12)$$

The total power dissipated in the strip is then:

$$dP_{FL}(x) = j_{mp}^2 R_{sh,FL} dx \int_0^{\ell} (\ell - y)^2 dy$$

$$= \frac{1}{3} j_{mp}^2 R_{sh,FL} \ell^3 dx \qquad (13)$$

As ℓ is a function of x:

$$\ell(x) = \frac{x}{W-x} h \bigg|_{x \le W-x_1} \quad \text{and} \quad \ell(x) = \frac{W-x}{x_1} \cdot h \bigg|_{x \ge W-x_1} \qquad (14)$$

it is:

$$P_{FL} = \frac{1}{3} j_{mp}^2 R_{sh,FL} h^3 \left\{ \int_0^{W-x_1} \frac{x^3}{(W-x_1)^3} dx \right.$$

$$\left. + \int_{W-x_1}^{W} \frac{(W-x)^3}{x_1^3} dx \right\}$$

and:

$$P_{FL} = \frac{1}{12} j_{mp}^2 R_{sh,FL} h^3 W; \qquad (15)$$

The derivation which is general with respect to the shape of the triangle, and its results (eq. 15) show that the Joule losses are independent of the particular shape of the triangle.

For the second type of approximation, a uniform current distribution is assumed to exist in a strip parallel to the grid line (Fig. 4). Thus, the power dissipated in the strip

16

located at the distance y from the grid line is expressed
by:

$$dP_{FL}(y) = I(y)^2 \, dR(y) \qquad (16)$$

As the current path is still assumed to be normal to the
grid line, it is:

$$dR(y) = R_{sh,FL} \cdot \frac{dy}{\ell(y)} ; \qquad (17)$$

and

$$I(y) = j_{mp} \frac{1}{2} \ell(y)(h-y) ; \qquad (18)$$

with:

$$\ell(y) = W \frac{h-y}{h} ; \qquad (19)$$

Thus:

$$dP_{FL}(y) = \frac{1}{4} j_{mp}^2 R_{sh,FL} \, \ell(y)(h-y)^2 dy;$$

and:

$$P_{FL} = \frac{1}{4} j_{mp}^2 R_{sh,FL} \frac{W}{h} \int_0^h (h-y)^3 dy;$$

$$P_{FL} = \frac{1}{16} j_{mp}^2 R_{sh,FL} \cdot h^3 W; \qquad (20)$$

The quality of the approximations is of some concern.
For the parallel grid line pattern, the front layer Joule
loss had been found to be:

$$P_{FL} = \frac{1}{3} j_{mp}^2 R_{sh,FL} \cdot \left(\frac{S}{2}\right)^3 W; \qquad (21)$$

for the rectangle of the front layer which is located on one
side of the grid line. The length $\frac{S}{2}$ corresponds to the height
h of the triangle on one side of the grid line in the fanned
pattern. As the total current from the rectangle is $j_{mp} \frac{S}{2} W$,
but that from the triangle only $j_{mp} \frac{h}{2} W$, a factor of $\frac{1}{4}$ for the
square of the total current should be expected, and consequently,
for the triangle, a Joule loss of:

17

$$P_{FL} = \frac{1}{12} \, j_{mp}^2 R_{sh,FL} \, h^3 \, W;$$

as in equation (16).

For the derivation of eq. (16), however, the assumptions of current flow normal to the grid line, and of a very non-uniform current distribution were made. It can be easily shown, that for a linear current distribution of the form:

$$I(x,y)dx = \left[ax + \frac{I(y)}{\frac{y}{h} W} \right] dx;$$

for
$$-\frac{y}{h} \frac{W}{2} \le x \le \frac{y}{h} \frac{W}{2}; \qquad (22)$$

with the total current I(y), the value of the square increases with the square of the slope a of the distribution. Thus, the square of the current is the smallest for the distribution assumed to be uniform according to Fig. 5. In this case, however, the current paths are longer than the assumed paths normal to the grid lines, so that eq. (20) would represent a lower limit for the actual Joule losses of the front layer. Equation (16), on the other hand, will probably be an upper limit, as the current distribution will not be as non-uniform as assumed there, but some of this reduction of the losses will be compensated by the actual longer current flow paths.

In any case, for the evaluation of the grid line pattern, the more optimistic values resulting from application of eq. (20) were used.

b. Results

The results of the calculations of the grid line losses for each grid line in the Westinghouse fanned grid line pattern, based on equations (2), (3), (9), and (20), are given in Table I, as well as their totals. It is seen that the approach of evaluating areas around all grid lines separately accounts for 18.08 mW of available power, while the available power based on the whole half-unit field area should have been 18.75 mW. The computed total relative power loss of 4.7% is based on the available power value of 18.75 mW.

For comparison purposes, a parallel grid line system has been evaluated with the same technology-based assumptions: sheet resistances of the diffused layer of 60 Ω, and of the grid lines (Cu, 8 µm thick) of $2.1 \cdot 10^{-3}$ Ω, and grid lines with uniform width of 25 µm. A four-line pattern on the half-unit field was found optimum under these constraints, with the geometry and the losses shown in Table II. These losses include both the shading and the Joule losses of a bus line, which should give a more direct redundant connection to the adjacent unit fields, and consequently a connection of lower resistance, than the continuation of the grid lines into the adjacent unit fields does in the fanned pattern. The parallel grid pattern also includes an interconnect attachment area identical to that of the fanned pattern.

In general, it can be concluded that the Westinghouse fanned grid line pattern design is a true low-loss metallization design. Nevertheless, a parallel grid line pattern can be used which performs at least equally well as the fanned pattern applying the same contact metallization technology constraints. Consequenlty, there is no performance uniqueness achieved with the fanned pattern.

TABLE I

WESTINGHOUSE FANNED GRID LINE PATTERN

LOSS CONTRIBUTIONS FOR HALF-UNIT FIELD

INPUT DATA:

R_{sheet}, FL = 60 Ω

Grid Lines: Width = 25 μm; Thickness 8 μm

Line #	P_{avail}	Shading Loss	Joule Losses		Total Loss	Relative Loss %
			Grid Lines	Front Layer		
1	2.475	0.0881	0.0259	0.0054	0.1194	4.82
2	2.475 (E)	0.0881 (E)			0.1194 (E)	4.82 (E)
3	2.475) E)	0.0881 (E)			0.1194 (E)	4.82 (E)
4	3.406	0.0896	0.0503	0.0167	0.1566	4.60 (E)
5	3.09	0.0533	0.0246	0.0293	0.1072	3.47
6	1.778	0.0296	0.0045	0.0182	0.0523	2.94
7	2.31	0.0184	—		0.1 (E)	4.3
Contact Pad	0.075	0.075	—	—	0.075	100
Sum	18.08	0.530			0.849	4.7
Unaccount'd	0.67					
Total	18.75					

All Numbers in mW

20

TABLE II

4 Grid Lines

25 μm x 8 μm
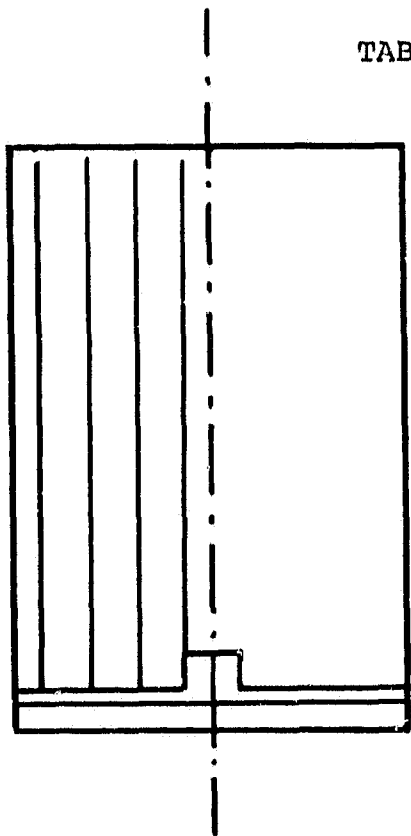
1 Bus Line

75 μm x 0.45 cm

$\frac{1}{2}$ Contact Pad

0.1 cm x 0.05 cm

$P_{avail} = 18.75$ mW

Shading Losses:

Grid Lines	0.3664 mW	
Bus Line	0.0521 mW	
Contact Pad	0.075 mW	
Total:	0.4935 mW	2.63 %

Joule Losses:

Front Layer	0.0768 mW	
Grid Lines	0.2186 mW	
Bus Line	0.0441 mW	
Total:	0.3395 mW	1.81%

Total Losses:	0.833 mW	4.45%

C. A Recommendation for Front Layer and Grid Line Pattern Design

An optimized grid line pattern design depends on the sheet resistance of the front layer, as it results from the diffusion or ion implantation process. Frequently, a particular grid pattern design is chosen based on the thought that this pattern might be easily fabricated in an available process. Subsequently, the cell performance is optimized by an empirical process of varying time and temperature in the diffusion process. This approach generally does not lead to an optimum design, since a compromise is struck between the influence of the front layer design on collection efficiency, open circuit voltage and fill factor. However, only the latter is influenced by the series resistance which results from the sheet resistance of the front layer and from the grid pattern design. The proper approach would be to first optimize the front layer formation process to attain the highest product of collection efficiency and open circuit voltage. In a second step then, a grid line structure should be designed so as to minimize the series resistance losses from both the front layer and the grid line pattern, and simultaneously the shading losses from the grid pattern.

II. SOLAR CELL DESIGN CONSIDERATIONS FOR FURTHER EFFICIENCY IMPROVEMENT

A. General.

All current cells employ, in the front layer, surface concentrations of the dopant impurity in the 10^{20} cm^{-3} range. It is well known that, in this concentration range, Auger recombination limits the minority carrier lifetime to values in the nanosecond range, while bandgap narrowing increases the saturation current and consequently reduces the open circuit voltage. The first is the major reason why present diffused layers have to be made so extremely thin, the second results in the present limitation of the open circuit voltages to the low six-hundred millivolt range, and both contribute to the formation of the so-called "dead layer" at the surface of the front layer.

A second part of the solar cell where heavy doping effects are frequently encountered, is in the so-called "BSF layer", if it is formed by diffusion or ion implatation. The BSF layers generated by these processes have been found to be far less effective than those resulting from the aluminum alloying process, primarily because of the heavy doping associated with the common use of these two processes, although the generally much smaller thickness of the highly doped layer between the high/low junction and the back contact which results from formation by these processes, would also reduce the effectiveness of the "BSF structure". However, with the limitation of the diffusion length to small values commensurate with the heavy doping, a thicker layer would not be more effective in this case. In the aluminum alloying process, the impurity concentration apparently is limited to $2 \cdot 10^{18}$ cm^{-3} by the solid solubility of the aluminum in silicon, with a consequently longer diffusion length, to which the greater thickness resulting from the empirically found alloying process is better matched.

For a future silicon solar cell of improved performance, heavy doping effects will need to be avoided in any part of the device. An exception might be a very thin layer just below the metallization, in order to facilitate the formation

23

of an ohmic contact. This very heavily doped and degenerate layer would then, in effect, form part of the ohmic contact, rather than an active semiconductor region.

With the reduced doping in the front layer, a resistivity up to 2 orders of magnitude higher than currently experienced will have to be expected. One order of magnitude in sheet resistance should be regainable by increasing the thickness of the front layer to 1 to 3 μm, as the avoidance of the heavy doping effects should yield a minority carrier lifetime 2 to 4 orders of magnitude higher than experienced in the present devices. This will still result in a front layer with a sheet resistance of 300-600 ohms. The proper reduction of the series resistance losses thus will require a fine line grid of about 10-25 μm line width with a line spacing of several hundred μm to a millimeter. The fabrication of such grid structures is well within the capabilities of today's technology, but may require the application of photolighography.

In addition to avoidance of the heavy doping effects, there will be a need for control of the surface recombination velocity on the open front surface. While a number of methods for surface passivation have been explored and applied in industry, it is not clear what effective surface recombination velocities are actually obtained. A question also arises relative to the results of some of the measurement methods applied. It will be necessary to pay more attention to the analysis and possibly the improvement of methods used for the determination of the front surface recombination velocity, which will be needed for the development of appropriate processes for its control.

There is another large area of a dependence of the solar cell performance achieved on the processes applied. This concerns the influence of the high temperature processes on the material parameters actually attained. A part of this question again concerns the front layer, this time with respect to the diffusion lengths which actually can be obtained by the processes

24

of diffusion, ion implantation, or CVD epitaxy. At least some of the processes used so far do not seem to be capable of attaining diffusion lengths comparable to those obtained in Czochralski or float-zone grown material of the same resistivity. There is the additional question of the introduction of defect centers which act as recombination centers both in the depletion region and the base region near the depletion region. In the depletion region, such centers would cause an excess dark current, as described by Sah, Noyce, and Shockley[11]. This excess dark current has found some study in the past and will require further investigation. If this dark current due to recombination in the depletion region is too large, it will degrade the fill factor. However, if the excess currents are negligibly small in the range of the IV-characteristic in which the current densities correspond to the maximum power in normal operating conditions, then a further reduction of these excess currents would not improve solar cell performance.

Some evidence has also been reported in the past that defects resulting from diffusion are introduced into the base layer near the depletion region. Findings have recently been reported by NASA-Lewis, that the mobility in the base may be substantially lower near the depletion region than it is at a greater distance from the depltion region[12]. This would be a surprising effect, since the mobility is generally less sensitive to defects than the minority carrier lifetime is. Consequently, if deleterious effects on the mobility have been discovered, it should be assumed that the lifetime would be even more strongly effected, with an influence both on the collection efficiency and the open circuit voltage. The NASA-Lewis people properly state that a mobility degradation near the depletion region would improve the open circuit voltage, but an accompanying influence on the minority carrier lifetime should well counterbalance this effect.
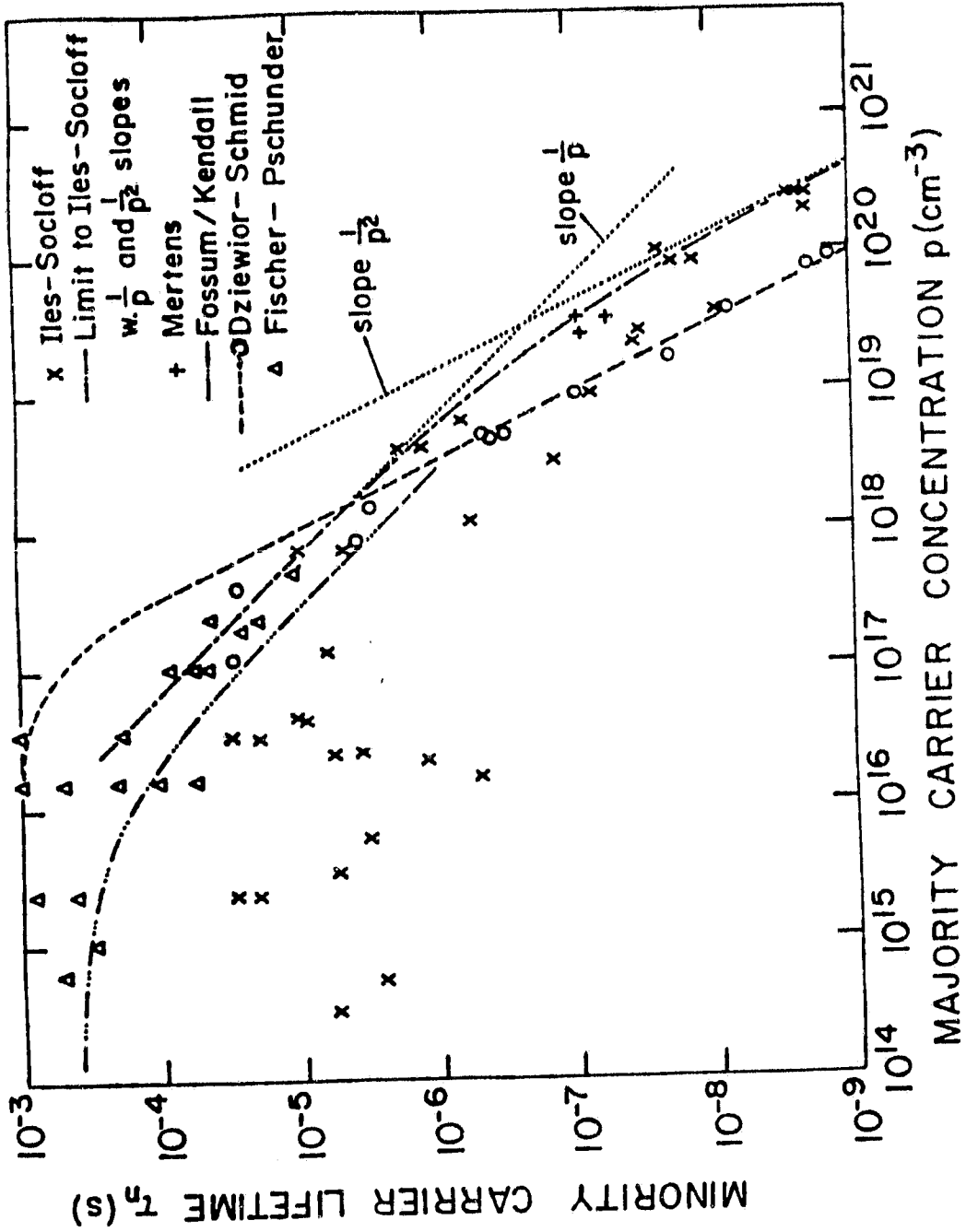
25

FIG. 6

B. The Dependence of Minority Carrier Lifetime on Carrier Concentration.

The values of the minority carrier lifetime, which can be expected to be obtained as function of the majority carrier concentration in silicon single crystal material were re-investigated in some detail through a literature study. Of particular interest are the limits of the achievable lifetime, including the question of direct band-to-band Auger recombination. As one result of this study, the data from various authors of minority carrier lifetime measurements as function of majority carrier concentration in p-type silicon were plotted together on the same graph (Fig. 6). These data include those by Iles and Socloff[13], by Kendall[14] in their interpretation by Fossum[15], by Dziewior and Schmid[16], by Fischer and Pschunder[17], and by Mertens et. al.[18]

Particular attention was paid to the data which were thought to represent direct band-to-band Auger recombination. This direct recombination does not involve any traps or recombination centers, and is therefore presently considered as the physical mechanism which fundamentally limits the minority carrier lifetime at high majority carrier concentrations. Auger recombination principally involves two majority carriers and one minority carrier, and its rate therefore depends by the inverse square law on the majority carrier concentration. The effective minority carrier lifetime, τ_{eff}, which is the result of two independent recombination mechanisms with the minority carrier lifetimes τ_1 and τ_2 occuring simultaneously, is given by:

$$\frac{1}{\tau_{eff}} = \frac{1}{\tau_1} + \frac{1}{\tau_2} \tag{23}$$

Auger recombination, with its $1/p^2$ dependence becomes the dominant recombination mechanism at adequately high majority carrier concentrations, and then determines the minority carrier lifetime τ_{eff}. As direct Auger recombination is a

fundamental mechanism not affected by defects or other process influences except the doping, it will determine the maximum attainable, or limiting minority carrier lifetimes. The Auger recombination is generally characterized by the Auger recombination coefficient C which is defined by the relationship

$$c_p = \frac{1}{\tau p^2} \tag{24}$$

for p-type material. A value for this coefficient has been theoretically found by tedious quantum-mechanical considerations, involving a number of assumptions. This theoretical value is therefore somewhat suspect. Dziewior and Schmid[16] have experimentally investigated Auger recombination in silicon by measuring the pulse of recombination radiation emanating from a wafer subsequent to the generation of minority carriers in it by the absorption of a strong photon pulse from a laser. Their lifetime data fall particularly well onto a $1/p^2$ line, and yield an Auger coefficient $C_p = 9.9 \times 10^{-32}$, in good agreement with the theoretically obtained value. A coefficient of this magnitude leads to the onset of the dominance of Auger recombination generally in the impurity concentration range of 10^{17} to 10^{18} cm^{-3}.

Other workers, including Iles and Socloff[13], Fossum[15], and Possin et. al.[19], have been discussing relationships between minority carrier lifetime and majority carrier concentration, which follow a $\frac{1}{p}$ dependency. While these authors do not try to relate the $\frac{1}{p}$ dependency to any particular physical model of recombination, Figure 6 shows that these dependencies may primarily apply in the majority carrier concentration range between 10^{16} and 10^{18} cm^{-3}, that is below the range in which Auger recombination is dominant. A $\frac{1}{p}$ dependency of minority carrier lifetime can be explained by Schockley-Read-Hall recombination if the recombination center is a very shallow trap. Shallow traps, on the other hand, are usually not considered as being very effective recombination centers,

so that this interpretation would require their presence in a high concentration. The levelling off of the minority carrier lifetimes towards still lower carrier concentrations, that is below 10^{16} cm^{-3} which is observed both in the Iles-Socloff and the Kendall data, could indicate that there is also a deep recombination center present, which would result in a recombination rate independent of the majority carrier concentration. This deep trap would have to be there in a lower concentration, so that it will determine the effective minority carrier lifetime only in the higher resistivity samples. This "apparent saturation" of the lifetime in the higher resistivity samples, which is seen to occur at differing values of the lifetime, could be explained by differing concentrations of the deep level trap present in the various samples.

Another interesting point concerns discrepencies in the experimental data at the high majority carrier concentrations. As explained above, Auger recombination should be the mechanism that poses the ultimate limitation to minority carrier lifetime at the high majority carrier concentrations. However, the data from Iles and Socloff as well as those of Mertens[18] substantially exceed the Auger limit found by Dziewior and Schmid in their carefully executed experimentation. The Iles-Socloff data are quite consistent with those of Mertens, and yield minority carrier lifetimes a factor of 20 larger than those thought possible according to the Dziewior and Schmid data. In addition, an investigation of high power transistor and thyristor structures by Possin, Adler, and Baliga[19] has found that the exact modelling which includes band-gap narrowing and Auger recombination, cannot explain the experimentally obtained data from collection efficiency measurements by the EBIC method carried out with a range of electron beam energies. The interpretation of the data would require the assumption of Auger recombination at least an order of magnitude smaller than that found by Dziewior and Schmid.

The question arises where the differences in the life-
time data from low resistivity material come from? One answer
could be doubts in the accuracy of the minority carrier life-
time measurements. Based on the general problems with minority
carrier lifetime measurements, and the usually experienced
discrepencies, such doubts are justified. A recent study by
this investigator has found that most of the minority carrier
lifetime measurement methods are afflicted with side effects,
which are usually neglected in the development of the theoreti-
cal background of the method, and which usually are also not
accounted for by the experimenter who applies the method.
This entire area of minority carrier lifetime measurements is
also one which will need considerable further attention.

While, in principle, all experimental data are somewhat
suspect, it is interesting to observe that the data with the
longer minority carrier lifetimes are all based on measure-
ments on completed devices, and may therefore include a greater
potential for unaccounted side effects. In contrast, the
Dziewior and Schmid data have been obtained on wafers, without
further processing or introduction of a potential barrier after
the growth and the cutting of the crystal. Also, the investi-
gation of the decay of the recombination radiation as performed
by Dziewior and Schmid is thought to be less susceptible to side
effects, than, e.g., the diode recovery method used by Iles
and Socloff. Also, the fact that the experimental results of
Dziewior and Schmid show only very small deviations from the
$1/p^2$ relationship conveys some confidence in the accuracy of these
data. On the other hand, the three investigators using devices
have applied completely different measurement methods as well as
different device structures, and have still arrived at results in
close agreement with the conclusion that the Auger coefficient
should be more than an order of magnitude smaller than that found
by Dziewior and Schmid. This agreement does not seem to permit
neglecting these data offhand. In fact, Possin et. al.[20]
outline a possible interpretation for the observed discrepancy:

It is known that trap assisted Auger recombination also exists, besides the direct band-to-band recombination discussed above. Both types of Auger recombination show the $1/p^2$ dependency. Thus, Dziewior and Schmid may have had samples in which trap assisted recombination was the dominant effect, rather than the direct recombination which they thought they were observing. In the preparation of devices, significant gettering can take place, so that the trap concentrations in the device samples could have been adequately suppressed so that the authors who investigated the devices and observed the longer minority carrier lifetimes, may actually have seen the direct band-to-band Auger recombination. Clearly, both explanations are sheer speculation at this time.

III. EVALUATION OF MINORITY CARRIER LIFETIME MEASUREMENT METHODS.

A. General

The preceding section has directed attention to the limitations of minority carrier lifetime measurements, and to the interpretation of data obtained in such measurements, in connection with the literature data on Auger recombination. There is an additional need for reliable minority carrier life-time measurements, namely for the determination of the minority carrier lifetimes actually achieved in the various layers of high efficiency solar cells, if the processing of these cells is to be controlled so as to yield the cell performance which is being predicted by modelling.

A large number of minority carrier lifetime or diffusion length measurement methods is in existence. Some of these methods are only minor variations from another method. In principle, the measurement methods can be divided into several categories. The first division may be into methods which are based on steady state (dc) phenomena, those, which are based on periodic (ac) phenomena, and those which are based on transient effects. The steady state methods generally determine the diffusion length rather than the minority carrier lifetime. The transient phenomena include effects such as recovery after a time period of excess minority carrier injection. A second broad categorization is based on the type of sample required. The first category uses a piece of plain semiconducting material, generally with at least 2 ohmic contacts. An example of such a method is the photo-conductive decay method. The second group requires the existence of a potential barrier in the sample, such as a pn junction or a Schottky barrier.

All the methods have been originally developed for a simplified case, which is relatively easy to model, and where the mathematics is tractable. The assumptions made to facili-tate such modelling vary somewhat from method to method, as do the effects which have been neglected. The problem is, that the

methods are frequently rather blindly applied, without attention
to their limitations, or the degree of conformity to the assump-
tions in the particular sample being investigated. The literature
is full of examples where such neglect is evident.

An effort has therefore been started to determine the
limitations of various minority carrier lifetime measurement
methods, and of the types and magnitudes of corrections to be
applied, as far as such corrections have been derived, or can
be derived. It can readily be seen that it is necessary for
the investigator of the minority carrier lifetime in a particu-
lar sample, to know the structure and the characteristics of
the sample in great detail before he can properly interpret the
data which result from the application of a particular minority
carrier lifetime measurement method. Only with such knowledge
can he apply the method in a range where disturbing effects
are least influential, and where he can interpret the results
of his measurements most meaningfully. Because of this consid-
erable influence of extraneous effects, at least 2 completely
different methods should be applied to any particular sample,
and agreement between the minority carrier lifetime data re-
sulting from these two different methods will be needed to
attain credibility for the data.

Of the numerous minority carrier lifetime measuring methods,
the storage delay time (diode reverse recovery time) method has
been studied in more detail for several reasons. It is a method
which has been very commonly used because it is easy to apply
with relatively inexpensive equipment. Many data in the lit-
erature, including those in several of the "Auger lifetime"
articles, were obtained by use of this method. Also, the equip-
ment for this method is available in this investigator's labo-
ratory, so that experiments can readily be carried out. The
method has, however, lately been touted as "unreliable",
although its limitations and problems of application and inter-
pretation may not differ much from those of most other methods.

Further, a Master degree student of this Principal Investigator has last year expanded the theory for the diode reverse recovery time or storage delay time (SDT) method for minority carrier lifetime determination to the case of arbitrary base widths with arbitrary surface recombination velocity at the plane boundaring the base opposite the pn-junction. All previous publications have dealt only with the cases of infinitely thick base regions [21, 22], or of infinite surface recombination velocity with arbitrary base widths [23-26].

However, the modern solar cells, containing in the base region a high-low junction and a third, more heavily doped layer of varying width, can exhibit a wide range of transport velocities through the interface plane between the first base layer and the high-low junction, depending on the design and quality of the high-low junction and the third layer. This transport velocity is equivalent to a surface recombination velocity at the back surface of a single layer base region.

In the real cases, both the bulk minority carrier lifetime and the transport velocity at the rear of the base layer are unknown. It will then be necessary to prepare several (at least two) samples with differing thickness of the base layer, but otherwise identical properties, to determine both the lifetime and the transport velocity.

With this new capability and the other positive attributes of the SDT method, a closer look seems indicated to determine its limitations, its range of applicability, and the precautions to be taken in its use.

B. The Storage Delay Time (Reverse Recovery Time) Method of
    Minority Carrier Lifetime Measurement.

This method belongs to the group which utilizes a transient
effect, and which requires a sample with a potential barrier,
usually a pn junction. A closely related method is the open
circuit voltage decay (OCVD) method. In one variant of the
latter, the same equipment is used as for the storage delay time
(SDT) method, so that both methods can easily be used in con-
junction with each other. Nevertheless, the OCVD method will be
discussed separately.

The SDT method is rather easy to use and not time consuming.
It requires only a fast switching device, two power supplies,
and an oscilloscope (Fig. 7). For the fast switching device,
a mercury wetted contact relay is frequently used, as it has no
contact bounce. In another variant which is better suited for
the measurement of very short storage delay times ($< 1\mu s$), a
power supply and a high power pulse generator are used.

The experimental procedure involves the measurement of the
storage delay time t_s on the oscilloscope display, after the
forward bias injection current I_f and the reverse bias recovery
current I_r have been appropriately adjusted (Fig. 8). If dis-
turbing electronic effects are present, such as significant
overshoots, pulse rounding, or ringing, they are displayed and
can either be abstracted by visual interpretation, if modest, or
be eliminated by improved circuit design.

The method has originally been derived[21, 22] under the
assumption of an abrupt, highly unsymmetrical junction, which
means that there is only insignificant injection into the more
heavily doped side of the pn junction, and consequently no sig-
nificant charge storage there. It has also been assumed that
the base region is infinitely thick, so that there is no influ-
ence of the boundary surface to the base opposite the pn junction.
As mentioned in the introduction, a number of workers[23-26] have
tried to expand the theoretical background to determine the re-
lationship between the measured storage delay time and the
minority carrier lifetime in the sample for the case of arbitrary

FIG. 7

FIG. 8

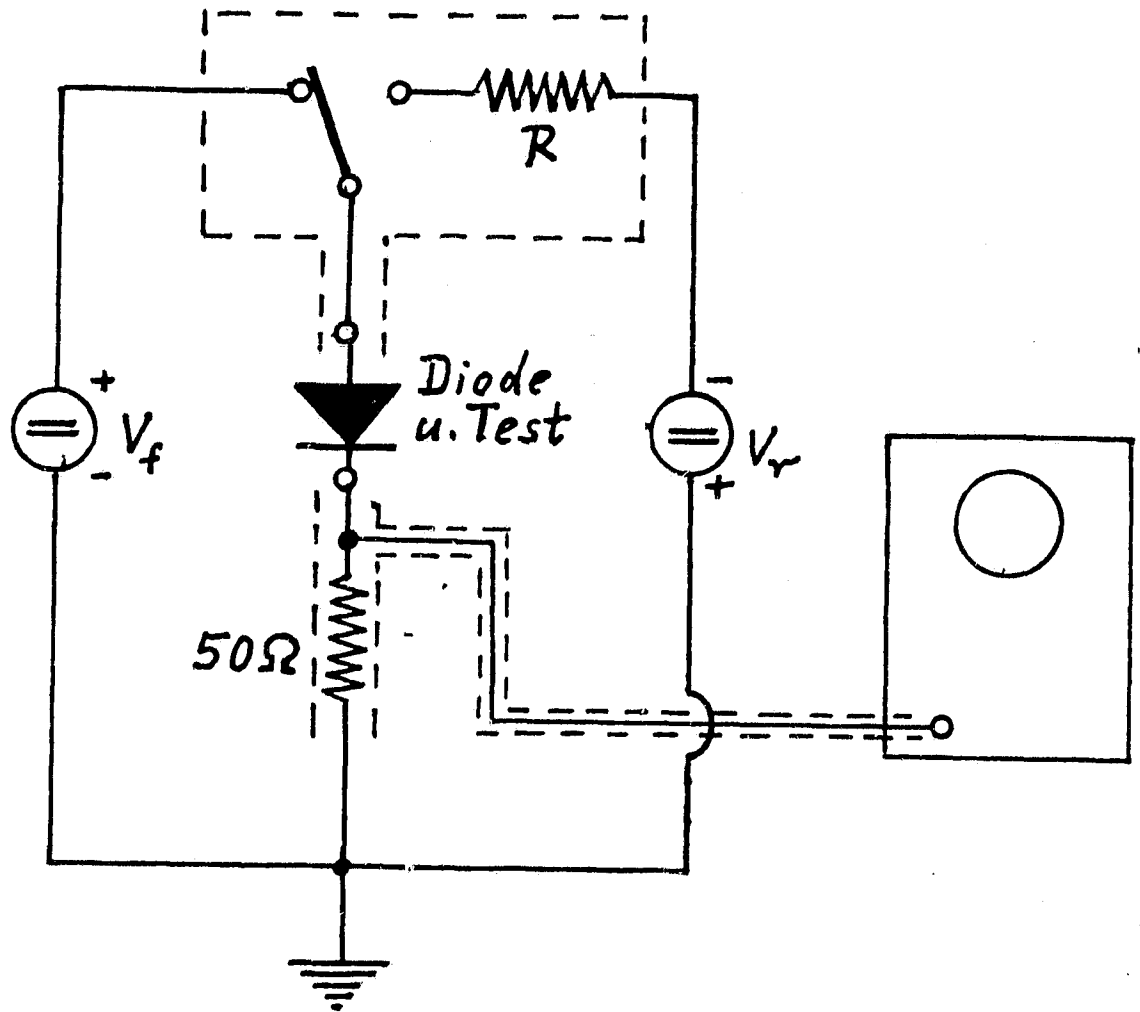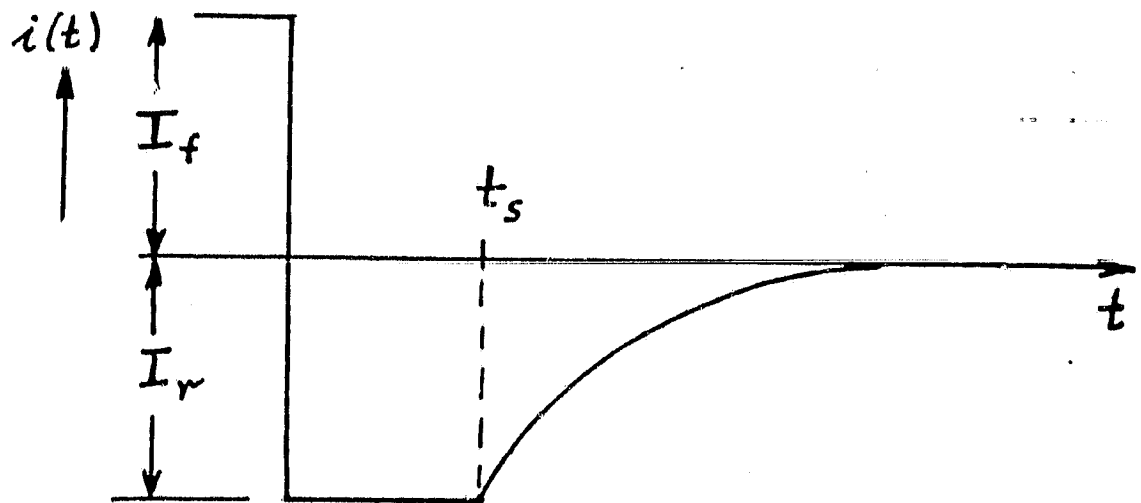base thickness, but with infinite surface recombination velocity
at the back surface.

In the SDT method, a steady state excess minority carrier
distribution is built up in the base region by injection of a
current across the pn junction with forward bias applied. For
the infinitely thick base, this distribution is a negative
exponential, with the excess minority carrier concentration
$n_p(x_{j,B})$ at the interface between the depletion layer and the
base $(x_{j,B})$ determined by the forward bias voltage V existing
across the depletion layer:

$$n_p(x_{j,B}) - n_{po} = n_{po}(e^{\frac{qV}{kT}} - 1) \qquad (25)$$

After switching at time $t=0$ from the injection condition
to the reverse bias power supply, the minority carrier distri-
bution in the base is initially the same as before, except for
an instantaneous change of the slope of the distribution at
$x=x_{j,B}$ from negative to positive, and a consequent minute change
in $n_p(x_{j,B})$. With $n_p(x_{j,B}, t=0^+) \simeq n_p(x_{j,B}, t<0)$ immediately
after switching $(t=0^+)$, the voltage across the depletion region
has also still to be the same with respect to sign, and only
minutely decreased in magnitude.

As time progresses, the excess minority carrier distribution
in the base will decrease for 3 reasons: 1. recombination in
the bulk of the base; 2. outflow of minority carriers into and
across the depletion region because of the large electric field
in this region (analogue: light generated current from base);
and 3. outflow of minority carriers through the rear boundary of
the base region, if the latter is less than a few diffusion
lengths thick. Consequently, $n_p(x_{m,B}, t)$ will decrease with
time, and so will the bias voltage V. The outflow of carriers
across the depletion region, and consequently the current I_r, is
limited by the resistance R. As the forward bias across the
depletion region is in the same direction as the power supply
voltage V_r, the voltage drop across the resistance R will be:

$$R \cdot I_r = V_r + V \simeq V_r \; ; \tag{26}$$

Eventually, $n_p(x_{j,B}, t_s) = n_{po}$ will be reached, and simultaneously $V=0$. From this point in time ($t = t_s$) on, the junction goes into reverse bias, although there is still stored charge in the base (Fig. 9). Thus:

$$I_r(t > t_s) = \frac{V_r - V}{R} < I_r (0 < t \leq t_s)$$

I_r decreases until it asymptotically reaches I_o.

During the entire process, the distribution of the excess minority carriers in the base changes, depending on the relative magnitudes of bulk recombination and outflows across the two base region boundary planes. In consideration of this change, the relationship between the storage delay time t_s and the bulk minority carrier lifetime τ_n in the infinitely thick base has been found to be[21, 22]:

$$\tau_n = \frac{1}{\left(\text{erfc} \frac{1}{1 + I_r/I_f} \right)^2} \cdot t_s \tag{27}$$

Streetman[27] has shown that the mathematical derivation can be greatly simplified when the assumption is made, in the case of the infinitely thick base, that the distribution will not change in time, but rather stay exponential. Then:

$$\tau_n = \frac{1}{\ln \left(1 + \frac{I_f}{I_r} \right)} t_s \tag{28}$$

For the usually applied case of $I_r = I_f$, the factor on t_s is 4.5 in eq. (27), and 1.44 in eq. (28), which is a very significant difference.

The method always involves the measurement of the time from the moment of switching to the end of the constant current phase, that is the "storage delay time". For a given sample, the
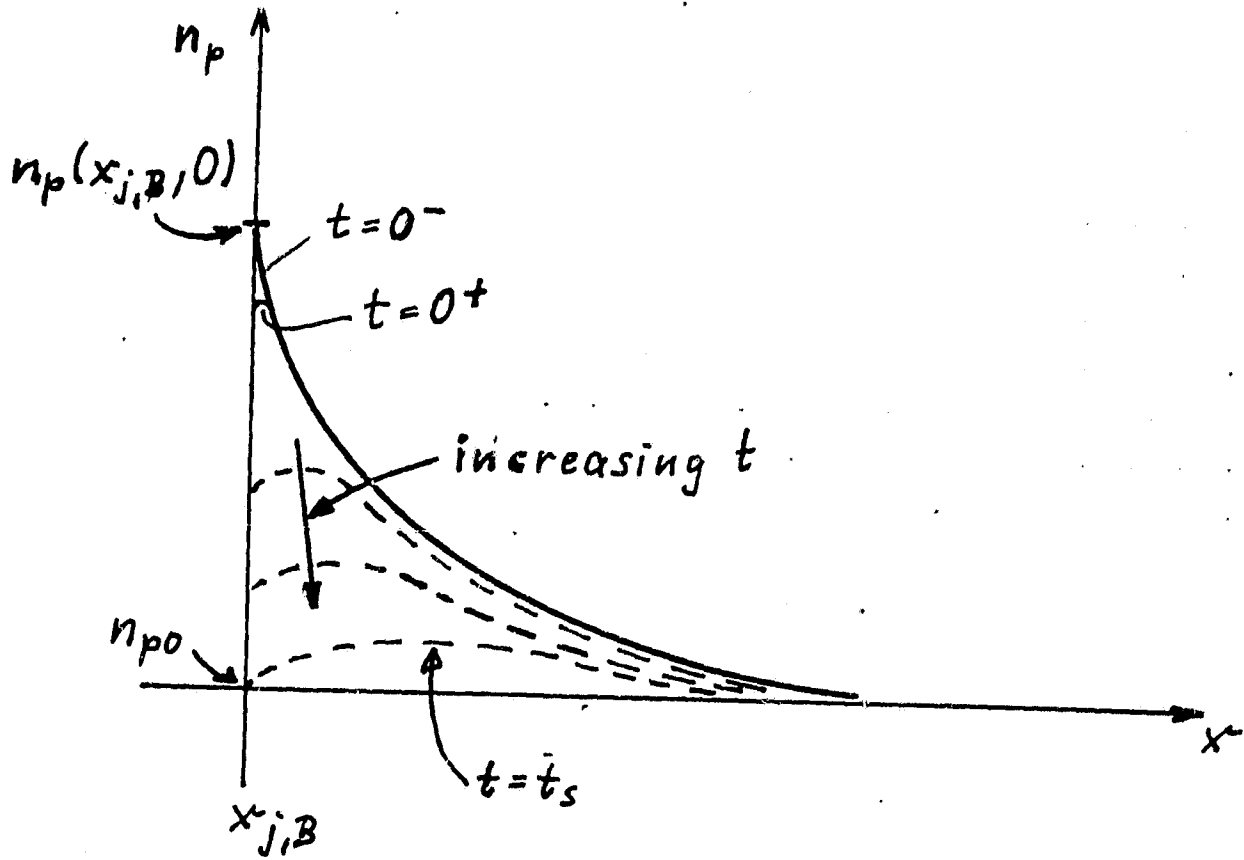
Figure 9

storage delay time varies according to the ratio of forward injection current to reverse recovery current. The relationship between the storage delay time and the ratio of the currents is given by eq. (27) only, if the diode is infinitely thick, and no other extraneous effects are present.

The limitations of the method are manyfold. The first limitation to be eliminated had been the restriction to large base widths, albeit only for the case of infinite surface recombination velocity at the back surface. In the last year, as mentioned before, the theory was expanded to include arbitrary surface recombination velocity with arbitrary base widths[28] (Fig. 10, 11). A problem is that, normally, the surface recombination velocity at the back boundary of the base layer is just as little known as the minority carrier lifetime. However, by preparing samples of varying base thickness, e.g. on the same wafer and with the same process, it should be possible to determine both the surface recombination velocity and the diffusion length in the base layer simultaneously. This would be of considerable benefit for the evaluation of solar cells which include high-low junctions. In these cells, it is important to determine the effectiveness of the high-low junction structure prepared, as well as the minority carrier lifetime effective in the base after all the applied processing.

There are several effects which can influence the determination of the minority carrier lifetime by the storage delay time (SDT) method. These effects can be grouped into two categories: first are influences on what appears to be the storage delay time resulting from the charge stored in the base. These influences result from the opposite side of the depletion region, (as seen from the base), from excess current due to recombination in the bulk or on the surface of the depletion layer of the pn junction, and from currents which result from the change of the depletion layer charge with varying junction voltage. The second group of effects includes those which are connected with the base region itself, but give rise to a base region "relaxation time" which does not equal the minority carrier lifetime
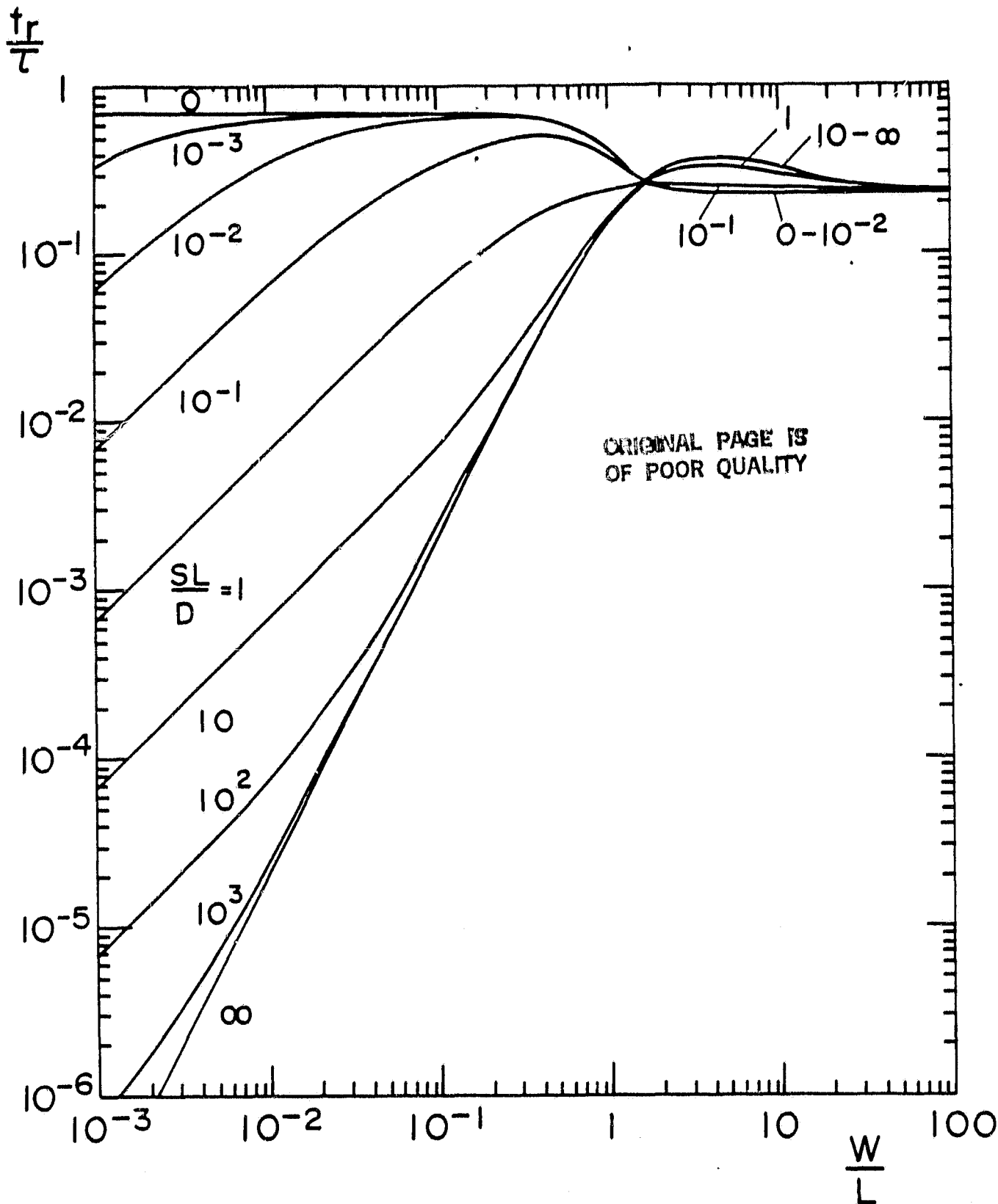
41

FIG. 10 : Dependence of the ratio of the recovery time to the lifetime on the ratio of the base width to the diffusion length for various values of the ratio of the surface recombination velocity to the bulk recombination velocity (the ratio of the diffusion constant to the diffusion length) for $J_f = J_r$.
(The data for Fig.10 and 11 were recalculated, with higher accuracy, after completion of the contract, and new figures representing the new data, were inserted in this version of the report.)

42
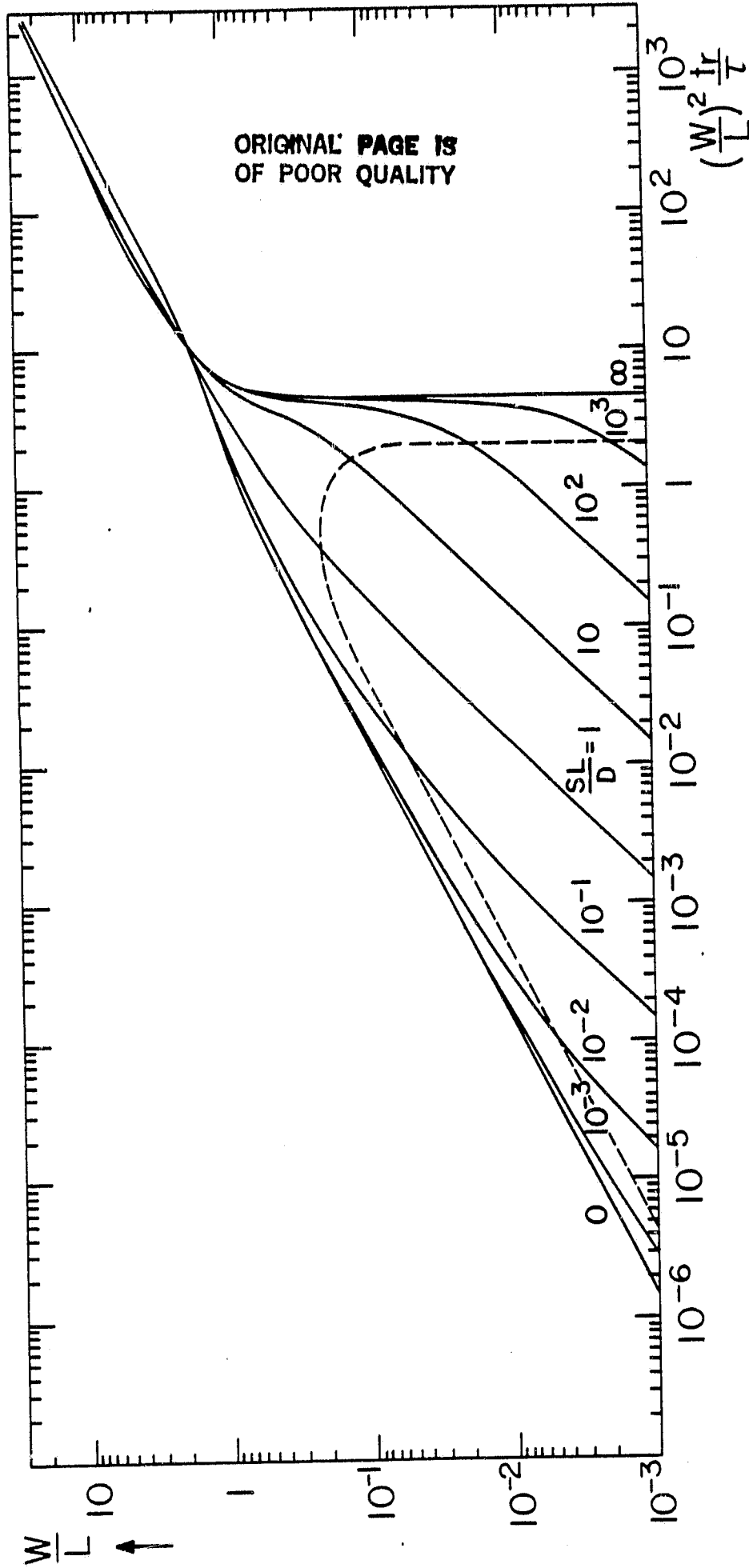
Dependence of W/L_p on the known quantity $\frac{W^2}{D_p} \cdot \frac{1}{t_r}$ for various values of $\frac{sL_p}{D_p}$.

(See note on Fig. 10.) The area below the dashed line represents the area where the lifetime is not determinable because of the dominance of the surface recombination velocity over the measured effects.

FIG. 11

in the bulk of the base region. These influences are the transport velocity out of the rear boundary surface of the base layer (frequently a surface recombination velocity), and the surface recombination velocity at the circumferential surfaces of the base layer.

The first severe criticism of the method was raised by Neugroschel et. al.[29] who pointed out that any significant charge storage on the opposite side of the pn junction from the base (they call it "emitter" although it may not have emitter properties) will influence the relationship between the minority carrier lifetime in the base and the measured storage delay time. They point out that the method really involves the determination of a "relaxation time" which includes the charge decay both in the base and the "emitter", but omit mentioning any back surface effects. They properly point out that the derivation of the method includes only the diffusion component of the diode forward current, and that therefore the measurement should be performed only in the region where the diffusion component determines the IV characteristics of the device. In real diodes, excess current results from recombination at the surface and in the bulk of space charge layers, particularly the depletion layer of the pn junction, and it is usually the dominant current in the low-voltage regime of the forward IV characteristic.

For a successful application of the method, therefore, the current voltage characteristic of the device to be tested has to be known and considered. Neugroschel et. al.[29] prefer the OCVD method over the SDT method, since they feel that the former is self-indicating if it is not carried out in the regime where the diffusion component dominates. However, if the SDT method is carried out at current levels where the excess current is negligible, it is fully valid, despite a statement to the contrary by Neugroschel et. al. Since the method is carried out with constant current flow, these current levels for I_f and I_r can, for many diodes and for most solar cells, easily be chosen so that they fall more than one order of magnitude above the excess current, while remaining in the "low-level" injection regime.

44

In the forward bias injection phase, any recombination
in the bulk or at the surface of the depletion layer results
in an "excess current" $I_{f,exc}$, by which the charge injected and
stored in the base region is reduced from that expected to
result from the measured forward injection current $I_{f,meas}$.
In the reverse bias recovery phase, the highest value of the
excess current $I_{r,exc}(t)$ will occur at the beginning of the
storage delay phase, as the excess current increases with for-
ward bias voltage, albeit less than the diffusion current does.
If this amount of excess current is neglible, then the sub-
sequently decreasing amounts will be negligible. It should be
noted that, during this phase, the extraction current is in-
dependent of the IV-characteristic, based solely on the stored
charge and its distribution, but limited by the external re-
sistor. Because of the still existing high carrier concentra-
tion in the depletion region (forward bias!), there occurs
still enhanced recombination there, which leads to a current
in the direction opposite to that of the extraction current,
and thus to a decreased value of I_r. Consequently, the measured
current values are:

$$I_{f,meas} = I_f + I_{f,exc} ; \tag{29}$$

and:

$$I_{r,meas} = I_r - I_{r,exc}(t) ; \tag{30}$$

As one adjusts $I_{r,meas}$ to be equal to $I_{f,meas}$, then one will
obtain:

$$I_r = I_f + I_{exc,f} + I_{exc,r}(t) \gtrsim I_f + I_{exc,f} ;$$

so that too short a storage delay time will be obtained. If
I_f cannot be chosen large enough to make $I_{exc,f} << I_f$ and
consequently negligible, knowledge of the IV characteristic
can permit a correction for $I_{exc,f}$ by setting:

$$I_{r,meas} = I_{f,meas} - I_{exc,f} = I_f \qquad (31)$$

This may permit acceptable measurements to be made in the range where $I_{exc,f} < I_f$, but not $I_{exc,f} \ll I_f$.

A second assumption usually made is that the charge change in the depletion layer is small compared to the charge stored in the base.[30]

As the depletion layer charge increases only with the square root of the applied bias, its effect can be made negligible by going to high enough current levels for the storage delay time determination, just as was found to be the case with the excess currents due to recombination in the space charge layer. The magnitude of the depletion layer charge can be determined either by a direct measurement of the junction capacitance, by calculation of the junction capacitance from known design parameters of the device - in either case at the values of applied bias at the beginning of the recovery phase and at its end - or from the decay phase following the recovery phase in the SDT method as suggested by Kuno's relationships.[31]

Practical application of the SDT method should consequently be preceded by an analysis of the IV characteristic of the device to be tested (Fig. 12 as an example) and a determination of the depletion layer charge. Figure 13 shows four storage delay traces of the 1cm x 2 cm Si n/p solar cell whose IV characteristic is shown in Fig. 12, taken at four different injection levels $I_{f,meas}$ for which the excess current is insignificant, as comparison with Fig. 12 indicates. At the three higher levels of the injection current, the same value of storage delay time is obtained, although the storage delay pulse becomes successively more rounded as the injection level is decreased. It may be noted that in all these cases, the low level injection condition is maintained. At the lowest injection level, however, the storage delay pulse is nearly completely obliterated by a "decay curve". This successive rounding and final obliteration is thought to result

46

FIG. 12

47

Solar Cell #51A — $I_f = I_r = 25\,mA;\; 2\,\mu s/div\; horiz.$

Solar Cell #51A — $I_f = I_r = 10\,mA;\; 2\,\mu s/div\; horiz.$
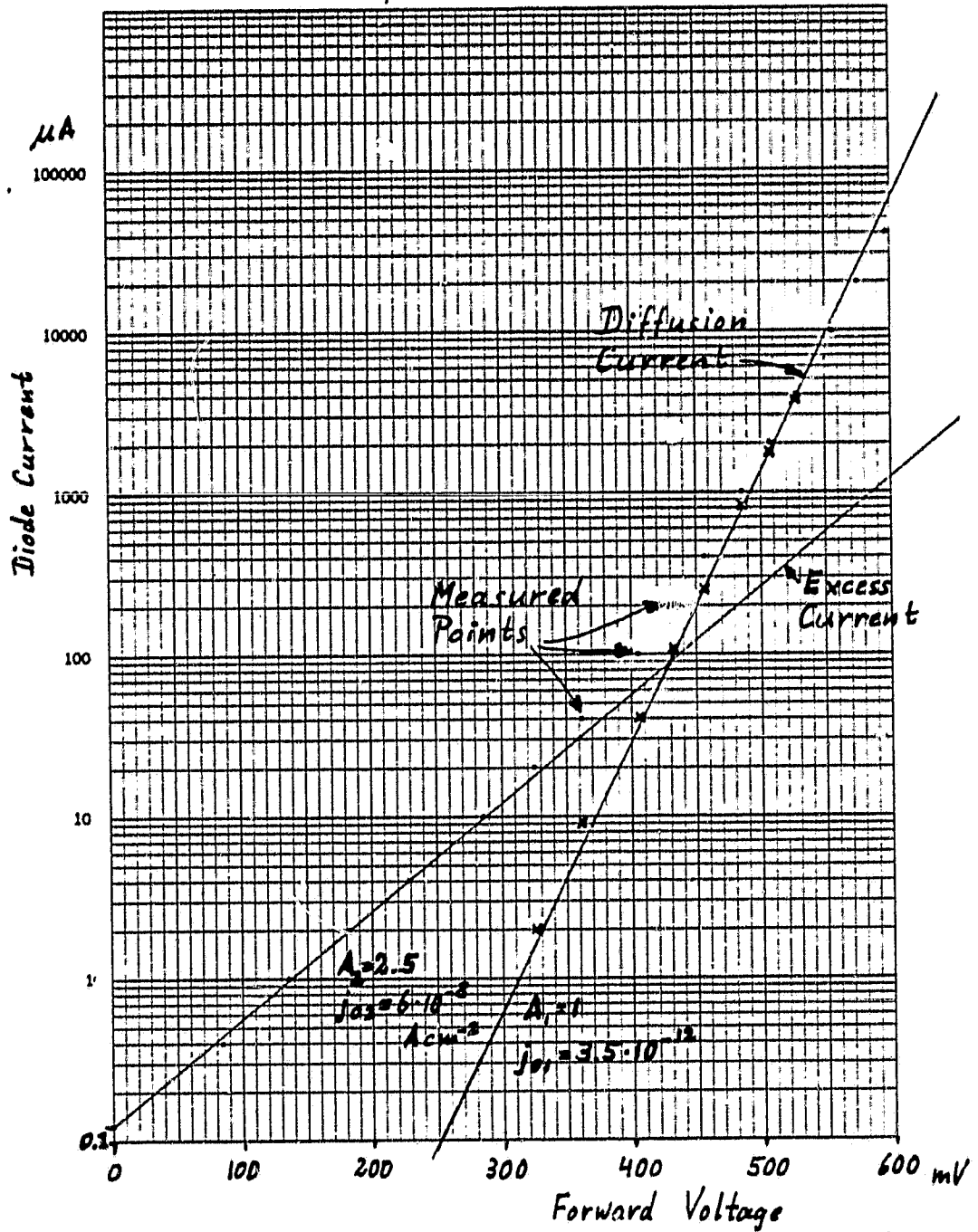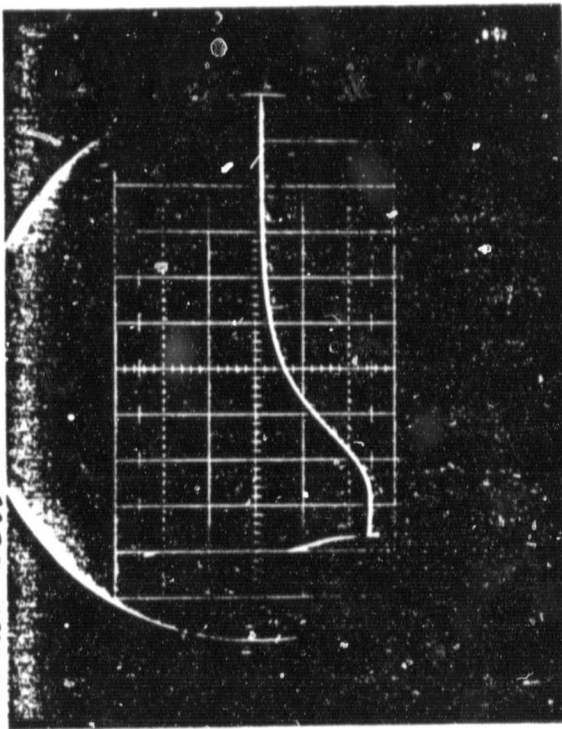
Solar Cell #51A — $I_f = I_r = 250\,mA;\; 2\,\mu s/div\; horiz.$

Solar Cell #51A — $I_f = I_r = 100\,mA;\; 2\,\mu s/div\; horiz.$
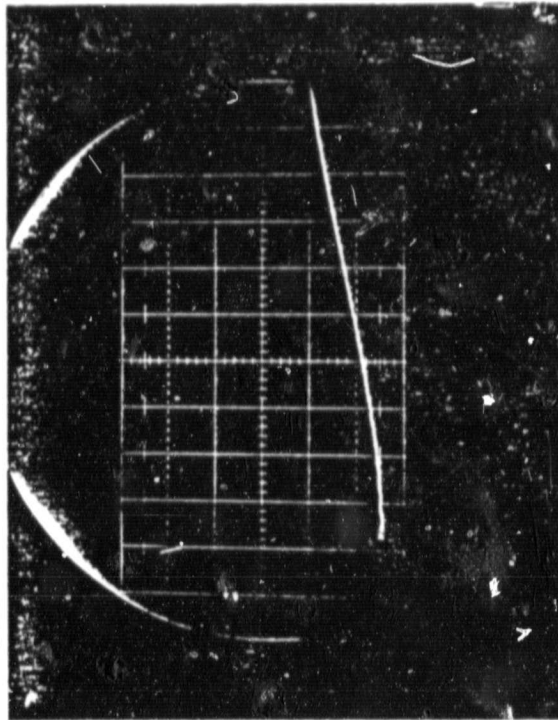
from the depletion layer charge, although this point is not proven. It cannot be the result of the excess current, but the change in depletion layer charge is of the same magnitude as the charge stored in the base at the lower injection level.

Finally, if the surface recombination velocity at the open surface at the circumference of the base layer is high, the excess minority carriers within approximately 1 diffusion length from this surface will diffuse to this sink rather than to the pn junction or the back surface. Thus, the existence of a high surface recombination velocity at the circumference of the base layer can have a significant influence on the relaxation time of the base layer, and consequently on the supposedly measured carrier lifetime for this layer.

1. Kuno's Modification of the Storage Delay Time Method.

Kuno has tried to simplify the theory of the SDT method, and to expand its application.[31] His extensive use of the charge control approach has made the analytical treatment appear very elegant, but has led to oversimplifications which, in the view of this investigator, have made his particular solutions useless for minority carrier lifetime determination.

Kuno has introduced the relaxation time τ_f which takes into account minority carrier bulk recombination in the base layer as well as transport out of this layer through its back surface. This relaxation time τ_f is a constant during the steady state part of the injection phase, but will generally not be constant during the recovery phase, as the carrier distribution in the base layer changes during the recovery phase, so that the ratio of the average minority carrier concentration in the base layer to the concentration at its rear boundary surface will vary in time. Consequently, the ratio of the bulk recombination to the transport out of this surface will vary during this phase, and with it the relaxation time τ_f. The exception is, when only bulk recombination is present, so that the relaxation time is constant. Treating this relaxation time as a constant, Kuno obtained an analytical solution to a differential equation for the total stored charge $Q(t)$ during the recovery phase with constant extraction current $-I_r$:

$$\frac{dQ}{dt} + \frac{Q(t)}{\tau_f} = -I_r \qquad (32)$$

The solution is:

$$Q(t) = (I_f + I_r)\ \tau_f\ \exp(-t/\tau_f) - I_t\tau_f \qquad (33)$$

With a non-constant relaxation time, the time dependence of the total stored charge should differ from the exponential, with an analytical solution not possible.

The second problem arises from Kuno's definition of the end of the storage delay phase. The time t_s is generally defined as the time from switching to reverse bias until the instant when the excess minority carrier density at the boundary surface between the base and the depletion region reaches zero. During this entire period t_s, the diffusion current due to the gradient of the excess minority carrier density in the base sustains the current $-I_r$, which is limited to this constant value by the external resistor R. Kuno defines the total charge stored in the base at time t_s by the expression:

$$Q(t_s) = I_r \tau_r \tag{34}$$

and replaces the proper boundary conditions

$$p(x_j, t_s) = 0 \; ; \tag{35a}$$

$$qD_p \left. \frac{dp}{dx} \right|_{x_j, t_s} = -I_r \tag{35b}$$

by eq. (34). He thus replaces the unknowns $Q(t_s)$ and t_s by the unknown time constant τ_r. By this approach he arrives at a relationship between t_s and τ_f:

$$t_s = \tau_f \left[\ln(1 + \frac{I_f}{I_r}) - \ln(1 + \frac{\tau_r}{\tau_f}) \right] \tag{36}$$

Plotting t_s against $\ln(1 + \frac{I_f}{I_r})$ should thus yield a straight line, with the slope τ_f and the intersect with the abscissa at $\frac{I_f}{I_r} = \frac{\tau_r}{\tau_f}$, as seen in Fig. 14.

The storage delay time was measured on a number of diodes and solar cells with varying values of I_f and $\frac{I_f}{I_r}$. Plotting t_s versus $\ln(1 + \frac{I_f}{I_r})$ has actually led to straight lines in many,

Solar Cell #54A

$\tau_F = \frac{t_b}{3} = 5.3 \mu s$

$\frac{\tau_R}{\tau_F} = 0.17$

$\tau_R = 0.9 \mu s$

taken at $I_R = 100 \text{ mA}$

$j_F = 50 \frac{mA}{cm^2}$

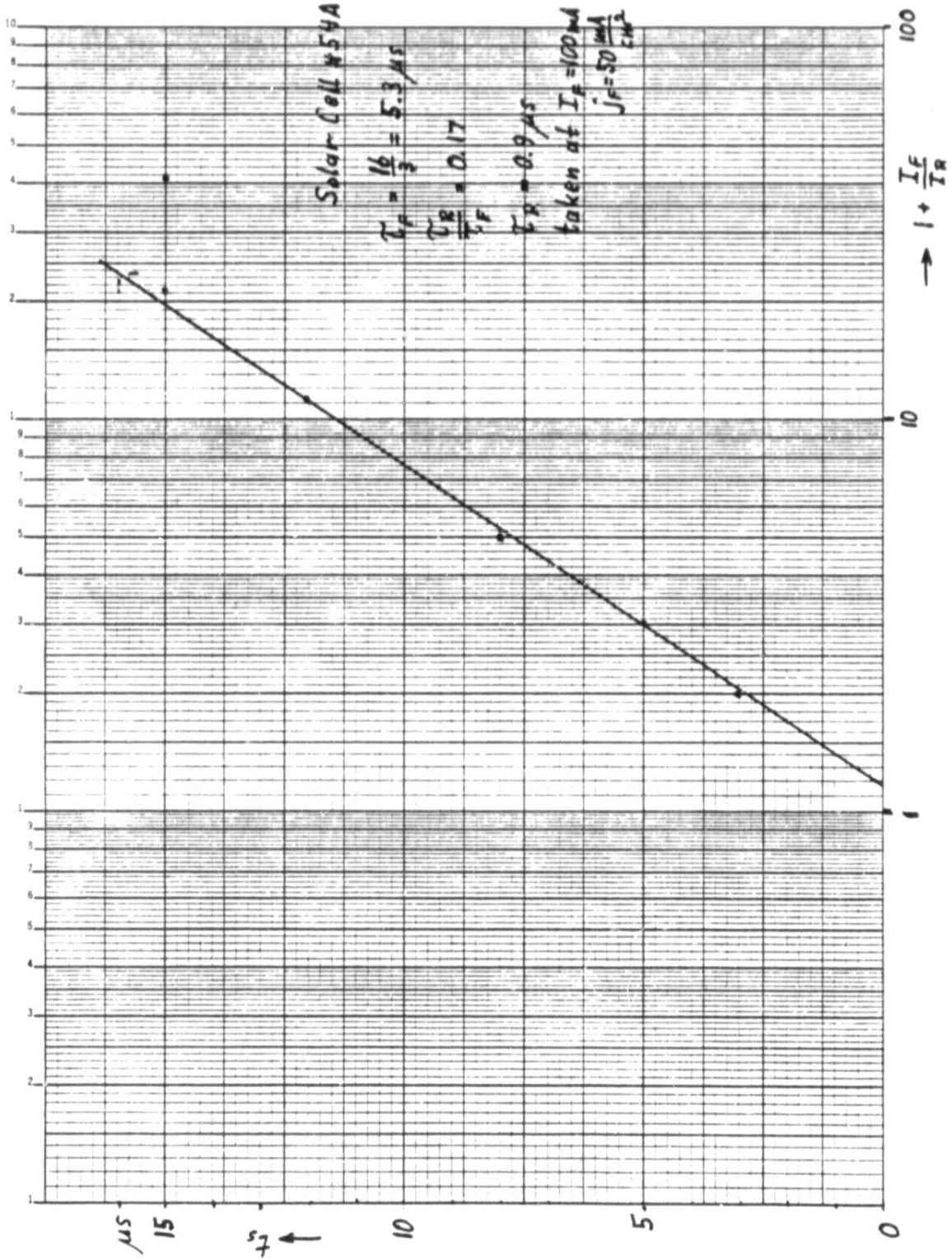$\longrightarrow 1 + \frac{I_F}{I_R}$

FIG. 14

52

but not all cases, but the values of τ_r obtained have all been small compared to τ_f, or actually zero. Consequently, the second term in eq. (36) has always been essentially zero, reducing the relationship between τ_f and t_s to the logarithmic relationship obtained by Streetman by assuming that the excess minority carrier distribution does not change during the recovery phase (eq. 28). Consequently, the minority carrier lifetime determined thusly is approximately a factor of 3 too small compared to the one obtained under consideration of the changing excess minority carrier distribution.

The problem evidently arises from Kuno's use of eq. (35) with various values of I_r, considering τ_r as a constant. In reality, $Q(t_s)$ will not be proportional to I_r at varying values of I_r, for values of t_s as usually defined, and as measured in the experiment. With τ_r = constant, a different $t_{s,Kuno}$ will be defined, which determines a $Q(t_{s,Kuno})$ according to eq. (35), but this $t_{s,Kuno}$ will not be measureable in the experiment.

Kuno extended his theory to also include the decay phase which follows the storage delay phase. While neglecting the effects of the depletion layer capacitance C_j during the storage delay phase, as have the previous workers, he has included its effect during the decay phase. Thus, he arrives at the relationship:

$$t_f = 2.3 \frac{\tau_r + RC_j}{1 + \tau_r/\tau_f} \tag{37}$$

for the measurable time t_f which he defines as the interval from the end of the storage delay phase ($t = t_s$) to the point where the current has been reduced to $0.1 \cdot I_r$. The capacitances obtained by this method were found to be about 50% higher than the zero bias capacitances calculated for the devices, while the actual effective capacitance during the decay phase should be less than the zero bias capacitance.
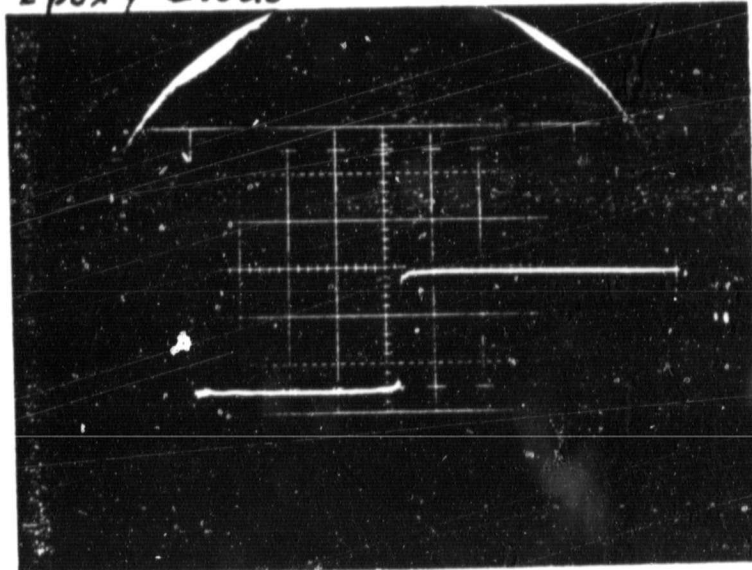
Epoxy Diode

$I_f = I_r = 100\,mA;\quad 1\,\mu s/div.$
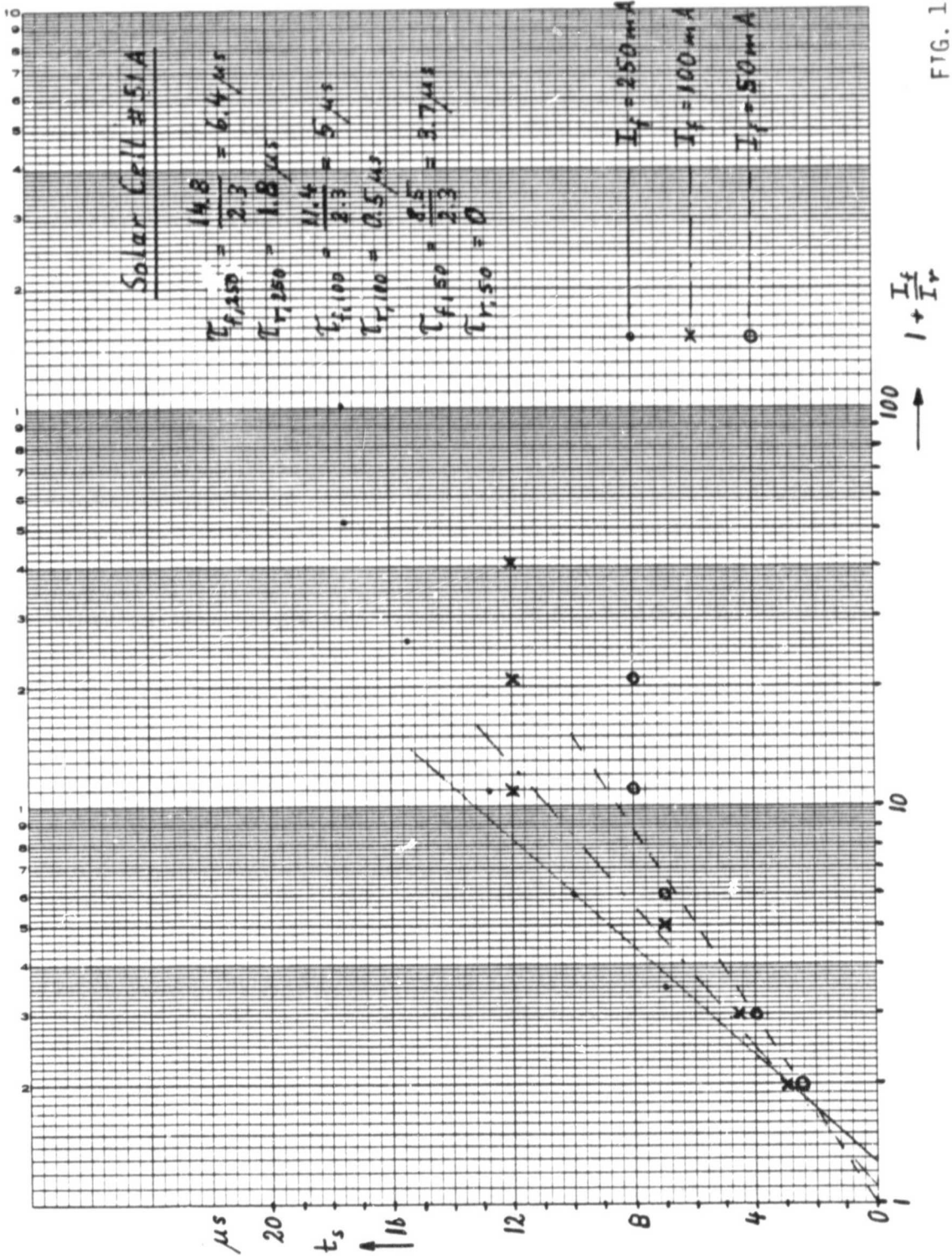
FIG. 15

FIG. 16

C. EXPERIMENTAL

The equipment for the determination of the dark IV characteristic and that for the observation and measurement of the storage delay effect, as well as for the OCVD method, have been assembled, carefully checked out, and debugged. They have been applied to a number of diodes which show a significant storage delay effect, as well as to several two ohm centimeter n on p silicon solar cells which were left over from an earlier experiment. At least one of these solar cells had been irradiated with low energy protons.

It is interesting to note that those of the diodes which exhibited significant storage delay effects, and which were available from supply, displayed strange IV characteristics. These characteristics seemed indicative of high level injection effects, as well as of narrow base effects. Apparently in consequence of the latter, the recovery characteristic shown in Fig. 15 was obtained, which exhibits an ideal recovery pulse with a negligible decay phase.

The solar cells, all of approximately 1cm x 2cm junction area, of either planar or conventional construction, with 2 Ωcm base layer and a p+ layer, when measured with $I_f = I_r = 250$ or 100 mA, showed a less square recovery pulse, and a significant decay phase (Fig. 13). At the current levels applied, both the excess currents and the depletion layer charge are an order of magnitude smaller than the injection current and the charge stored in the base, respectively (Fig. 12). The "Kuno interpretation" of a number of storage delay time measurements on this cell at three levels of I_f, and with varying I_f/I_r ratios, gave neither credible straight lines, nor the same slope τ_f or time constant τ_r for the three injection levels (Fig. 16). In addition, the fall time t_f increased from 7 μs to 20 μs with increasing I_f/I_r ratio from 1 to 50, at $I_f = 250$ mA, with a similar behavior observed at $I_f = 100$ mA.

The smallest value of fall time t_f in the decay phase, 7 μs, together with the largest value of τ_r, 1.8 μs, resulted in the capacitance value C_j = 44 nF. This value compares with the measured zero bias capacitance value of 68 nF, and the calculated value of 52 nF, for a rather good agreement in this particular case.

The minority carrier lifetime in the base would be 13.5 μs according to the Kingston theory for the infinitely thick base. The Kuno interpretation gives < 6.4 μs, and OCVD resulted in 1.6 μs. With $\mu_n \simeq 1200$ cm^2 V^{-1} s^{-1}, the diffusion length with 13.5 μs lifetime would be $L_n \simeq 200$ μm. With a cell thickness of about 300 μm, and a high/low junction present, the "infinite base" approximation is questionable. Such questioning is particularly justified, as the measured saturation current density j_{01} would demand a twofold larger diffusion length, or a five times larger minority carrier lifetime than obtained from the Kingston method. This difference is not readily explained.

IV. CONCLUSIONS

A review of the MEPSDU metallization processes has indicated that the Solarex grid pattern design and process selection, in combination, lead to excessive Joule and shading losses, while the Westinghouse metallization system is as close to optimized as can be expected. In addition, it is not clear that the Solarex front layer diffusion process and the BSF formation process are actually optimized.

A study of the minority carrier lifetimes, achieved in various samples, in dependence on the impurity concentration has led to three primary conclusions. First, further investigation and refinement of the various minority carrier lifetime measurement methods and of their interpretation is required. Second, a further study of Auger recombination is needed, until the Auger coefficients for both trap-assisted and direct recombination are conclusively determined by application of differing methods. Third, some device processing methods are deleterious to the minority carrier lifetime, while others may include adequate amounts of gettering so as to improve the minority carrier lifetime by an order of magnitude or more relative to that found in the as-grown and cut samples. Since the minority carrier lifetime is one of the key parameters which determine the efficiency available in silicon solar cells, more studies will have to be performed to understand the influences on the minority carrier lifetime which is exerted by the various processing methods available.

An additional, but probably less urgent conclusion is, that the ultimate determination of the direct Auger recombination coefficients will lead to a review of the optimum design for the solar cell. If the Auger coefficients should actually turn out to be more than an order of magnitude smaller than the presently accepted value, the design of the solar cells would be changed in the direction of utilizing higher impurity concentrations,

with corresponding adjustments in the device structure so as to achieve an additional efficiency gain.

An investigation of minority carrier lifetime measurement methods has led to the conclusion that all methods are afflicted by 2 sources of errors: effects which lie outside of the portion (such as the base layer of a diode) of the sample for which one wants to determine the minority carrier lifetime; and effects which originate from the desired portion of the sample, but which alter the "signal" which would be attributable only to the bulk minority carrier lifetime. Most prevalent among the latter are surface recombination effects, while for measurements on devices with a potential barrier, excess currents and depletion layer charges are frequent sources of error from the first group. To arrive at credible data, a great deal needs to be known about the attributes of the sample to be tested, and considerable sophistication exercised in the execution and interpretation of the measurements.

REFERENCES

1. Solarex Quarterly Report No. 1; pp. 82-88; DOE/JPL 955902-81/1, Nov. 1980 to Feb. 1981,

2. Solarex Quarterly Report No. 2, pp. 14-15; DOE/JPL 955902-81/2, Mar. to May 1982.

3. Solarex Quarterly Report No. 1, p. 66; Table I, "Price Estimates Using IPEG Approximation", DOE/JPL 955902-81/1, Nov. 1980 to Feb. 1981.

4. Solarex Quarterly Report No. 2, pp. 26-34; DOE/JPL 955902-81/2, Mar. to May 1981.

5. Ibid., pp. 20-25.

6. Ibid., pp. 11-16.

7. Solarex Quarterly Report No. 3, pp. 8-22; DOE/JPL 955902-81/3, May to Aug.1981.

8. Solarex Quarterly Report No. 2, pp. 16-17; DOE/JPL 955902-81/2, Mar. to May 1982.

9. Westinghouse Quarterly Report No. 3, p. 17, DOE/JPL 955905-81/3, June to Aug. 1981.

10. R.A. Davis, private communication

11. Shah, C.T., Noyce, R.N., and Shockley, W; Proc. IRE 45, p. 1228, (1957).

12 Weizer, V.G., Godlewski, M.P., and Trivisonna, R.J., Record of the 15th IEEE Photovoltaic Specialists Conf., pp. 892-897, IEEE Cat. No. 81CH 1644-4, May 1981,

13. Iles, P.A., and Socloff, S.I., Record 11th IEEE Photovoltaic Spec. Conf., IEEE Cat. No. 75CH0948-OED, pp. 19-24, May 1975.

14. Kendall, D., Conf. Physics and Applic'n. of Lithium Diffused Silicon, NASA Goddard SFC, Dec. 1969.

15. Fossum, J.G., Sol. St. Electronics, 19, pp. 269-277, 1976.

16. Dziewior, J., and Schmid, W., J. Appl. Phys. Letters 31, pp. 346-348, Sept. 1, 1977.

17. Fischer, H., and Pschunder, W., Rec. 11th IEEE Photovoltaic Spec. Conf., IEEE Cat. No. 75CH 0948-OED, pp. 25-31, May 1975.

18. Van Meerbergen, J., Nijs, J., Mertens, R. and Van
    Overstraeten, R., Rec. 13th IEEE Photovoltaic Spec. Conf.,
    IEEE Cat. No. 78CH1319-3, pp. 66-69, June 1978.

19. Possin, G.E., Adler, M.S., and Baliga, B.J., IEEE Trans.
    El. Dev., ED 27, pp. 983-990, 1980.

20. Adler, M.S., and Possin, G.E., IEEE Trans. El. Dev., ED-28,
    pp. 1053-1059, 1981.

21. Kingston, R.H., "Switching Time in Junction Diodes and
    Junction Transistors", Proc. IRE 42, pp. 829-834, (1954).

22. Lax, B., and Neustadter, S., "Transient Response of a pn
    Junction", J. Appl. Phys. 25, pp. 1148-1154, (1954).

    Lederhandler, S.R., and Giacoletto, J.J., "Measurement of
    Minority Carrier Lifetime and Surface Effects in Junction
    Devices", Proc. IRE 43, pp. 447-483, (1955).

23. Byczkowski, M., and Madigan, J.R., "Minority Carrier Life-
    time in pn Junction Devices", J. Appl. Phys., 28,
    pp. 878-881, (1957).

24. Grove, A.S., and Sah, C.T., "Simple Analytical Approximations
    to the Switching Time in Narrow Base Diodes", Sol.
    St. Electronics 7, pp. 107-110, (1964).

25. Davidson, L.A., "Simple Expression for Storage Time of
    Arbitrary Base Diode", Sol. St. Electronics 9, pp. 1145-
    1147, (1966).

26. Lewis, D.C., "On the Determination of the Minority Carrier
    Lifetime from the Reverse Recovery Transient of pnR Diodes",
    Sol. St. Electronics 18, pp. 87-91, (1975).

27. Streetman, B.G., "Solid State Electronic Devices", Problem
    5.16, p. 204; Prentice-Hall, Englewood Cliffs, NJ, 1972.

28. Hoffer, R.D., "Effects of Surface Recombination Velocity
    on Minority Carrier Lifetime Measurements by the Diode
    Reverse Recovery Time Method", Thesis for the Master of
    Science in Engineering for Electrical Engineering and Science,
    University of Pennsylvania, August 1981.

29. Neugroschel, A., Lindholm, F.A., and Sah, C.T., "A Method
    for Determining the Emitter and Base Lifetimes in pn Junction
    Diodes", IEEE Trans. El. Dev., ED-24, pp. 662-671, (1977).

30. Dhariwal, S.R., and Vasu, N.K., "A Generalized Approach to
    Lifetime Measurement in pn Junction Solar Cells", Sol.
    St. Electronics 24, pp. 915-927, (1981)

31. Kuno, H.J., "Analysis and Characterization of PN-Junction
    Diode Switching", IEEE Trans. El. Dev. ED-11, pp. 8-14, (1964).